Chapter 9

Nanostructured Spinel Ferrites: Synthesis, Functionalization, Nanomagnetism and Environmental Applications

Oscar F. Odio and Edilso Reguera

Additional information is available at the end of the chapter

http://dx.doi.org/10.5772/67513

Abstract

Nanostructured spinel ferrites have gained a great deal of attention. It comes from the possibility of tuning their magnetic properties by careful manipulation of the synthetic conditions. At the same time, since the nanoparticle (NP) surface is reactive toward many chemical groups, it provides great versatility for further functionalization of the nanosystems. Such characteristics make ferrite nanoparticles excellent candidates for environmental applications. First, the chapter deals with the basics of the synthetic methodologies, functionalization strategies and magnetic properties of nanoparticles, with emphasis on how surface manipulation is reflected in the properties of the materials. Next, we review some of the applications of ferrites as magnetic sorbents for several hazardous substances in aqueous medium and try to systematize the adsorption mechanism as a function of the coating material. Finally, a short summary concerning the main uses of ferrites as magnetic catalysts in oxidation technologies is included.

Keywords: spinel ferrites, superparamagnetism, surface complexes, heavy metals, dyes

1. Introduction

Magnetic nanoparticles (NPs) have been the focus of intense studies, both at the fundamental and at the technological level. Among many promising materials, nanostructured spinel ferrites occupy a special place. These iron oxide-based materials are easy and cheap to synthesize, are stable under a wide range of conditions and some family members present low toxicity for living organisms. Besides, due to their high reactivity toward several organic groups, ferrite surface offers a great versatility for ligand functionalization, which in many cases defines the ultimate application. In addition, one of the most prominent properties of spinel ferrite NPs is

the onset of superparamagnetism. This phenomenon is a crucial feature for several biomedical applications [1], catalytic processes [2, 3] and environmental remediation strategies [1, 4–7]. Currently, there are available in the literature several extensive reviews covering these issues in detail [8, 9]. In this chapter, we focus primarily on adsorption and oxidation technologies for water decontamination using nanostructured spinel ferrites where particle functionalization plays a major role. In particular, we focus on basic topics concerning spinel ferrite NPs with an emphasis on the surface manipulation by chemical methods and how it is reflected in the properties and performances of the ultimate nanomaterial. Also, attention is paid to the machinery that governs the adsorption process in order to try to systematize the available data. Every step in this direction is aimed to improve and design newer and better solutions for the great challenge of water remediation.

2. Structural and magnetic properties

Spinel ferrites are mixed valence oxides where oxygen anions form a close-packed cubic array, while metallic cations occupy randomly one-eighth of the tetrahedral (**A**) sites and one-half of the octahedral (**B**) interstices. This family is classified into the *Fd3m* space group with the general formula $[M_{(1-i)}Fe_i]^A[M_iFe_{(2-i)}]^BO_4$, where M (Fe, Ni, Mg, Mn, Zn, Co, etc.) is a divalent cation that shares with Fe(III) cations the occupancies of **A** and **B** sites, while *i* is defined as the inversion parameter. There are three possibilities [10]: (i) $i = 0$ yields a *normal* spinel such as $ZnFe_2O_4$; (ii) $i = 1$ yields an *inverse* spinel such as Fe_3O_4 and $CoFe_2O_4$ and (iii) for $0 < i < 1$ cations are distributed on both sites yielding a partially inverted spinel such as $MnFe_2O_4$ in which $i = 0.2$. In addition, it is possible to synthesize mixed ferrites in the sense that different divalent cations could coexist in the same compound [11, 12]. All these possibilities open an amazing range for tailoring different properties [11, 13].

In the spinel structure (left panel of **Figure 1**), magnetic moments of sublattice **A** are coupled with magnetic moments of sublattice **B** in an antiferromagnetic fashion by superexchange interactions mediated by the oxygen anions [14]. Since spins in both lattices are generally uncompensated, the resulting net magnetic moment causes the material to display ferrimagnetic behavior [10]. As can be inferred, either the type of divalent ion or the average ion distribution plays a critical role in the magnetic properties of the material. This effect can be illustrated by varying the Zn content in the mixed $Zn_xFe_{3-x}O_4$ ferrite [11] in which Zn^{2+} presents a zero magnetic moment ($\mu = 0$) and a high tendency for tetrahedral **A** sites. In the interval $0 < x < 0.4$, the saturation magnetization (M_S) increases as x increases, since the antiferromagnetic **A**-**B** interaction is progressively weakened, thus enhancing the net magnetic moment in sublattice **B** (see the right panel of **Figure 1**). However, for values of x near 1, **A**-**B** interactions are no longer dominant, but the magnetism now depends on the very weak **B**-**B** interactions, thus leading to a marked decrease of M_S, which becomes zero at $x = 1$.

2.1. Nanomagnetism

Magnetic NPs differ from bulk magnetic materials mainly due to the finite size and surface effects. The reduction of size leads to a single magnetic domain at a particular size and the onset

http://dx.doi.org/10.5772/67513

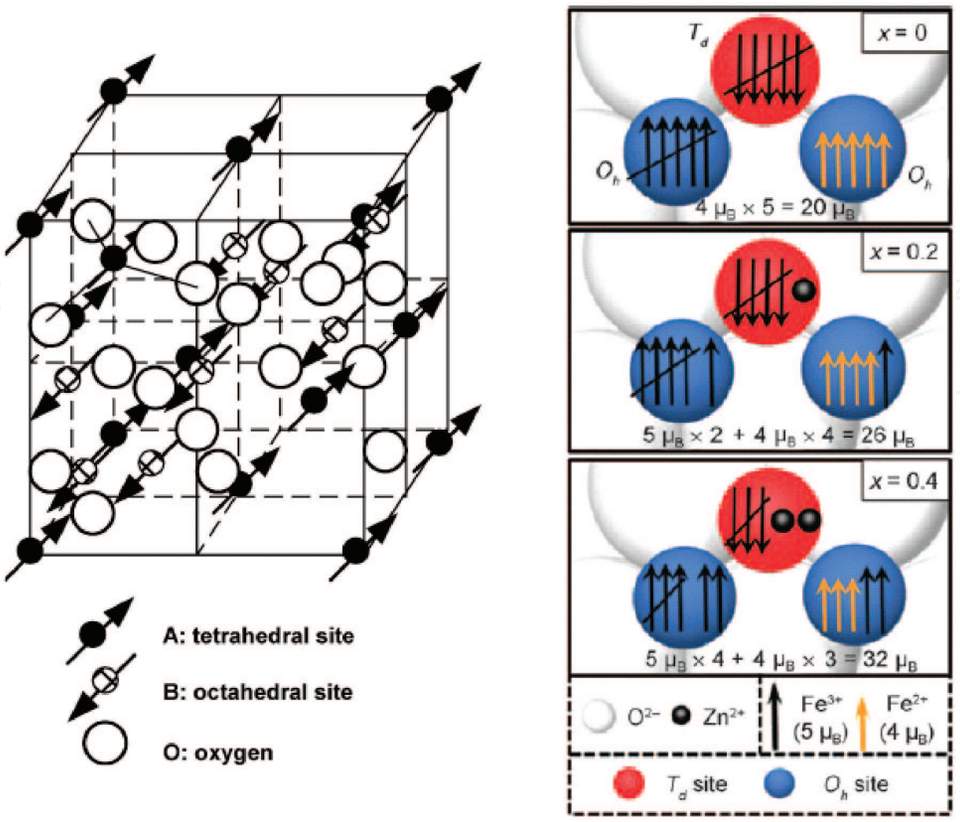

Figure 1. *Left:* Representation of a partial spinel ferrite unit cell and the ferrimagnetic order of the structure (Reproduced from Ref. [10] with permission of the American Society of Chemistry). *Right:* Schematic view of the spin organization in sublattice **A** and **B** as a function of the content of Zn in $Zn_xFe_{3-x}O_4$ (Adapted from Ref. [11] with permission of Wiley).

of superparamagnetism, while surface effects result in symmetry breaking of the crystal structure, which could also alter the magnetic properties. These new features are treated briefly below.

2.1.1. Single-domain limit

Large magnetic particles usually have a multidomain structure, each domain separated from its neighbors by domain walls. As the particle diameter D or volume V is decreased, domain wall creation is no longer energy favorable for a specific size, leading to single-domain NPs with all atomic spins aligned in the same direction. This critical particle diameter is characteristic for each material and is of the order of tens of nanometers (128 nm for Fe_3O_4) [9]. Since the spins are parallel within the NPs, magnetic reversal does not depend on wall displacement but is only possible by the coherent rotation of spins, which depends entirely on the effective anisotropy (K_{eff}). Given that coercitivity (H_C) is proportional to K_{eff}, it is higher for nanomaterials with respect to their bulk counterparts. For single-domain particles with uniaxial anisotropy, the anisotropy energy is defined as:

$$E(\theta) = K_{eff} V \sin^2\theta \tag{1}$$

Here, θ is the angle between the net magnetization and the easy axis of magnetization. For spherical particles, K_{eff} can be expressed as:

$$K_{eff} = K_V + \frac{6}{D} K_S \tag{2}$$

Here, K_V and K_S are the volume and surface anisotropies, respectively. As can be seen, for ultra-small NPs, the surface term may dominate the total anisotropy of the material.

2.1.2. Superparamagnetism

The product $K_{eff}V$ is the energy barrier for the coherent rotation of all atomic spins between the two equivalent easy axes of magnetization. As D is decreased, the thermal energy k_BT eventually overcomes the energy barrier for a particular size, thus leading to thermal equilibrium of the total magnetic moment of the system. In this state, the resulting H_C is zero and the system behaves like a paramagnet but with a huge magnetic moment. For an assembly of non-interacting single-domain NPs, each magnetic moment fluctuates with a relaxation time τ given by the Arrhenius-Néel law [15]:

$$\tau = \tau_0 e^{(K_{eff}V/k_BT)} \tag{3}$$

Here, τ_0 is a characteristic time of the system and the actual magnetic state at a given T depends on the measuring time τ_m. If $\tau < \tau_m$, the systems are in the superparamagnetic state, and for $\tau > \tau_m$, the spins appear in a blocked state. The temperature for which $\tau = \tau_m$ is the so-called blocking temperature T_B and is given by:

$$T_B = \frac{K_{eff}V}{k_B} \ln \quad (\tau_0/\tau_m) \tag{4}$$

One of the main advantages of ferrites is the possibility for tuning the magnetic properties by varying simply either the divalent cation or the arrangement of the metals into the spinel structure. For instance, in a series of nanoparticle ferrites MFe_2O_4 (M = Mn^{2+}, Fe^{2+}, Co^{2+}, Ni^{2+}, Zn^{2+}), Mohapatra *et al*. [16] could vary M_S and T_B by taking advantage of the differing magnetic moments and spin-orbit coupling strengths of M^{2+} cation. Similar conclusions can be extracted from other reports [17]. Likewise, for ultra-small $CoFe_2O_4$ NPs, the progressive variation in the inversion index (from a total to a partially inverted spinel) as D decreases is reflected in a decrease in the magnetocrystalline anisotropy and hence, in the H_C of the material [18]. In other works, Tahar *et al.* [13] found that as Zn^{2+} substitutes Co^{2+} cations in 5-nm-mixed $Zn_xCo_{1-x}Fe_2O_4$ ferrite NPs both H_C and T_B decrease, in accordance with progressive reduction of magnetocrystalline anisotropy, which is higher for octahedral coordinated Co^{2+} cations.

2.1.3. Surface effects

Progressive decrease in NPs' size makes the number of atoms on the surface comparable with the number of atoms in the bulk. For magnetic NPs, this trend lowers M_S and increases K_{eff} as D decreases [19, 20]. The decrease in M_S is associated with the presence of a magnetic dead layer, occurrence of spin canting or spins glass-like behavior at the surface level. The increase in K_{eff} is associated with the onset of surface anisotropy following Eq. (2).

The effect of surface coating in order to tune the magnetic properties of NPs is another area of active investigations. The adsorption of organic ligands could alter the particle size distribution, the interparticle interactions and the spin canting at the surface [21]. The overall effect seems to be the result of a complex interplay between the coordination mode, the capping density and the surface disorder in the synthesized sample [22]. In a careful study of adsorption of stilbene carboxylates and phosphonates as capping agents of 39 nm Fe_3O_4 NPs, Daou *et al.* [23] reported that carboxyl ligands tend to enhance spin canting at the surface of the oxide, leading to M_S reduction; on the other hand, phosphonate ligands seem to mimic the iron coordination in the bulk, hence, M_S of the NPs is unaltered as for uncovered Fe_3O_4. However, a direct correlation between magnetic measurements and the nature of the coordination bonding at the organic-inorganic interface is still needed. Regarding the important case of carboxylates, Odio *et al.* [24] found that spin disorder is larger in chelating than in bridging complexes; it suggests that occurrence of this last geometry makes possible the partial reconstruction of the crystal field of iron ions in the bulk phase. In another report, Aslibeiki *et al.* [25] noted that tetraethylene glycol ligands attached to Fe_3O_4 surface also contribute to decrease the surface spin disorder. Similarly, Jia *et al.* [26] noted that in Co- and Ni-mixed ferrite with SO_4^{2-} attached to the surface, M_S values increase with the content of superficial anions. In contrast, adsorption of carbonyl groups belonging to poly(vinyl pyrrolidone) (PVP) capping chains of Mn ferrites seems to decrease M_S values [27].

In an interesting paper, Vestal and Zhang [28] performed a systematic study of the correlation between the nature of the capping ligand (substituted benzenes) and the magnetic properties of $MnFe_2O_4$ ferrites with different particles' diameter. They found that for very small NPs (4 nm), H_C is reduced by ligand interaction with respect to the uncovered ferrite, while M_S is enhanced. Such behavior is consistent with the fact that metal-ligand interactions at the surface reduce K_S, leading to a reduction of H_C, and at the same time, they induce spin order at the surface. Furthermore, the authors showed that the higher the crystal field splitting energy of the surface complex, the smaller the magnitude of the spin-orbit interaction parameter and hence, the smaller the K_S value. The fact that such trends are less pronounced for larger particles (12 nm and 25 nm) reveals the importance of surface effects in H_C and M_S of single-domain NPs. This point has been verified in other reports [16, 29]. Besides, the contribution of K_S to K_{eff} is revealed when comparing the H_C variation of $MnFe_2O_4$ and $CoFe_2O_4$ particles with the same diameter and organic ligands: in the case of Co ferrite, the larger magnetocrystalline anisotropy masks K_S variation, leading to nearly unchanged values of H_C [30].

2.1.4. Magnetic interparticle interactions

The presence of magnetic interactions between particles has a great influence on superparamagnetism [31–33]. This effect alters the energy barrier for coherent rotation, which is no longer governed by only anisotropic contributions. The system becomes very complex and results in the difficulty to separate the contributions of different factors [34]. For ferrite NPs, the ordinary kinds of magnetic interactions are dipolar-dipolar and direct exchange interactions between spins at the interface of particles in close contact [35]. The first contribution is almost ubiquitous in any system, given its anisotropic and long-range nature, which could favor either ferro or antiferromagnetic alignment of the spins. The minimization of such an

effect can only be achieved in samples where individual particles are well separated from each other, either by steric or by coulombic repulsions [25, 36]. The dipolar magnetic field generated by a single spherical particle is proportional to its volume; hence, the effect is more pronounced for large particles. In that case, the magnetic energy between two spheres decays with d^{-3}, but smaller systems in the superparamagnetic state (where moments fluctuate) partially destroy the order induced by dipolar interactions, and hence, the energy associated decays with d^{-6}. In the limit of strong interactions, particles do not relax according to their own energy barrier, but the magnetic evolution depends on the energy of the whole ensemble [22, 34, 36, 37].

In the presence of interparticle interactions (IPI), Eq. (4) for T_B is modified to [38–40]:

$$T_B = To + \frac{K_{eff}V}{k_B}\ln\left(\tau_0/\tau_m\right) \tag{5}$$

Here, $T_o < T_B$ is a measure of the strength of the IPI in the system. To determine T_o, T_B needs to be measured at several different measuring frequencies $f_m = 1/\tau_m$. The presence of IPI is also determined by the quantity $\Phi = \Delta T_B/[T_B \Delta \log_{10} f_m]$ with $\Delta T_B = T_B(2) - T_B(1)$ being the difference in T_B determined at two sufficiently different measuring frequencies $f_m(2) > f_m(1)$ [41]. The magnitude of $\Phi < 0.13$ signifies the presence of IPI with its strength increasing with decreasing magnitude of Φ. In a recent paper [42], Φ and T_o have been shown to be related by the equation:

$$\Phi = \Phi_o\left[1 - \left(T_o/T_B(1)\right)\right] \tag{6}$$

In Eq. (6), $\Phi_0 = 2.3026/\{\ln[f_0/f_m(2)]\}$. As noted above, measurements of T_B at several different frequencies are essential in order to determine K_{eff} since f_o and T_o must also be determined simultaneously [40].

3. Synthesis

Synthesis of spinel ferrite NPs is a challenging task owing to their colloidal nature. A good methodology must yield well-dispersed particles with uniform size and good crystallinity; besides, it is desirable that the synthetic setup allows for the tuning of structure and properties of the materials by simple modification of the conditions. Other important features entail the use of nontoxic reagents, low-temperature processes and the requirement of simple scalable operations. The procedures for the synthesis of ferrite NPs are given in several reviews [2, 8]. Here, we outline some of the most common examples.

3.1. Co-precipitation

Co-precipitation is straightforward and efficient and can be extended for a wide variety of simple and mixed ferrites [12, 43, 44]. This method, developed by Massart, consists of the joint precipitation of an aqueous solution containing inorganic salts in the proper stoichiometry by increasing the solution pH. Ageing of the resulting particles can be assessed at room or higher temperatures. By changing experimental conditions (e.g., concentration of metal precursors, pH of the final solution, anion of initial salts, reaction time, reaction temperature and ionic

http://dx.doi.org/10.5772/67513

strength), it is possible to obtain a wide variety of particle sizes and shapes [45, 46]. The main drawback relies on the difficulties for a proper separation of nucleation and growth stages, which leads to relative broad size distribution [45]. Besides, in some instances, the resulting powder is subjected to thermal annealing to enhance crystallinity [12, 43].

Nucleation and growth of NPs can be affected by the addition of surfactant molecules like sodium dodecyl sulfate [47], poly(acrylic) acid (PAA) chains [48] and hexadecyl trimethylammonium bromide (CTAB) [49]. Variations in the surfactant content give rise to different particle sizes and morphologies of the as-synthesized material. Other employed additives aiming to decrease the particle size dispersion are polymeric matrices like cellulose [50] and chitosan [51, 52]. A similar approach entailed the use of graphene oxide (GO) during the co-precipitation step. After the formation of the ferrite/GO composite, GO is reduced to yield porous nanocomposites containing superparamagnetic ferrite NPs and reduced GO (rGO) is used as a functional material. The resulting material possesses high surface area since rGO avoids ferrite particle agglomeration. Ni, Co and Mn ferrites/rGO nanocomposites have been synthesized with this strategy [53–55]. Alternatively, some investigations have reported the use of organic amines, which can act as precipitating and stabilizing agents [17, 56, 57]. Alkanolamines limit and control the particle growth by forming surface complexes with M^{2+} cations resulting in a marked reduction in Co ferrite size as compared when using NaOH [56].

3.2. Thermal decomposition

This method utilizes thermal decomposition of organic metal complexes in a high boiling point solvent and in the presence of a surfactant. This approach yields monodisperse highly crystalline NPs and allows for the fine-tuning of NP size and morphology by controlling several parameters like the solvent nature, kind and concentration of surfactant, aging temperature and reaction time. The typical setup with oleic acid (OA)/oleylamine (OAm) as surfactants can be used to obtain $(Zn_xM_{1-x})Fe_2O_4$ ($M = Fe^{2+}$, Mn^{2+}) mixed ferrites with different Zn contents as the doping cation [11]. OAm is believed to assist OA deprotonation, which promotes the formation of iron carboxylates at the NP surface [58]. In a systematic study, Mohapatra *et al.* [16] have reported the synthesis of MFe_2O_4 ($M = Mn^{2+}$, Co^{2+}, Fe^{2+}, Ni^{2+}, Zn^{2+}) NPs using chloride salts as precursors and OAm acting as a solvent, reducing agent and stabilizing surface capping agent. By decreasing the amine content, it was possible to obtain uniform NPs with *D* values between 2 and 9 nm. OAm chains seem to control the growth process: high concentration enables an extended coverage of the initial nuclei, which hampers a fast growth and leads to uniform small NPs.

In an important report on the synthesis of Fe_3O_4 and other ferrite NPs, Hyeon *et al.* [59] used iron(III) oleate as an organometallic precursor with the purpose to avoid environmental harmful reagents like $Fe(CO)_5$ [60] and $Fe[acac]_3$ [61]. Also, there is no need for external reducing agents and extra surfactant stabilizers [36, 61–63]. The authors obtained high yields of well-crystallized monodispersed NPs with *D* values ranging from 9–22 nm by varying the solvent boiling point. Moriya *et al.* [64] introduced an interesting approach in which a pre-synthesized trimetallic complex containing two Fe^{3+} cations and one divalent cation (Fe, Co, Mn) is decomposed in dibenzyl ether in the presence of benzylic acid (BA). The resulting nanocrystals showed uniform size with variable shapes (from truncated octahedrons to cubes) that can be

tuned as BA concentration is increased; the nature of the weak intermolecular interactions between adsorbed BA molecules seems to play a key role to bring about the final morphology.

One drawback of the thermal decomposition method is that the as-synthesized ferrite NPs do not disperse in water due to the hydrophobic surfactant adsorbed onto the surface, which leads to further phase transfer steps. To obtain directly water-soluble NPs, the groups of Li [29] and Verma [58] introduced a variation in which 4–5 nm Fe and Co ferrites are obtained through the decomposition of metal acetylacetonates in the presence of pyrrolidones that act either as solvents or as hydrophilic stabilizing agents.

3.3. Polyol method

This is a variation of the thermal decomposition in which a given polyol acts as a high-boiling solvent, reducing and stabilizer agent. Metal precursors are generally organic complexes like acetylacetonates and other carboxylate complexes [65]. Given that the reaction mixture is refluxed at the boiling point of the polyol, changing either the kind or concentration of the polyol leads to different particle *D* values [66–68], generally between 4 and 15 nm. The obtained NPs have a narrow size distribution and high crystallinity, although particle agglomeration could occur. There is question about the nature of the molecules adsorbed at the particle surface; some authors have stressed that polyol anchoring to the surface occurs through R-O^- interactions [69, 70], but others have claimed that at high temperatures, hydroxyl groups are oxidized to carboxylic acids, which are further adsorbed onto the oxide surface by forming carboxylate complexes [71]. In many applications, there is no need for further treatment, since the NPs are stable in polar solvents [71]; however, in order to increase water stability and avoid particle aggregation, several polymers can be added to the reaction mixture like PVP and poly(ethylene imine) [67]. Many approaches also include functional materials like carbon nanotubes (CNT) in order to yield magnetic composites with enhanced properties [72]. This method has been used for Fe_3O_4 as well as for other nanospinels such as Co and Zn ferrites [13, 18, 70, 73].

3.4. Hydrothermal and solvothermal synthesis

Hydrothermal methodology consists of the formation of an aqueous (or aqueous-alcoholic) solution of the metal salts followed by the addition of a base until basic pH is reached. The resulting mixture is then transferred to a pressurized autoclave and subjected to $T > 180\,^{\circ}C$ for many hours. The mechanism involves the initial formation of metal hydroxides, which are oxidized and converted into the crystalline spinel ferrite due to the thermal treatment at high pressures. The resulting NPs have high crystallinity and an acceptable narrow size distribution. Particle size and shape can be effectively tuned by varying the metal concentration, solvent composition, temperature and reaction time. The addition of surfactants like CTAB [74] and poly(ethylene glycol) (PEG) [75] can change the shape of NPs and aid to control the growth and avoid agglomeration. This method can be adapted for the in situ synthesis of ferrite composites with functional materials like rGO [76, 77]; after base addition, metal hydroxides are adsorbed onto GO, and both spinel crystallization and GO reduction (by the action of supercritical water) occur during hydrothermal treatment. As a result, the size of near-spherical Zn ferrite NPs decreases as the GO content increases. On the contrary, the absence of GO sheets yielded NPs with a rod-like shape [78]. An alternative procedure by Komarneni *et al.* [79] involves hydrothermal treatment under microwave

radiation, leading to a drastic reduction in reaction times to just few minutes; this approach was useful for many ferrites.

Solvothermal synthesis can be understood as a modified hydrothermal process where water is replaced by an organic solvent. For instance, n-octanol along with sodium dodecylbenzenesulfonate has been employed for the preparation of mixed ferrite NPs of Ni and Co with several compositions and varying sizes (7–16 nm), which was tuned as a function of the reaction time [26]. OA can also be used as a steric stabilizer in the reaction mixture using n-pentanol as a solvent [22]; increasing OA content decreases *D* from 19 to 5 nm and changes the particle morphology from nanoplatelets to well-dispersed nanospheres. Other approaches reported the use of diol molecules as solvents [25, 80, 81]. Bastami *et al.* [80] introduced PEG and PVP as polymeric surfactants, which bind preferentially at the surface of the near normal (i = 0.2) $MnFe_2O_4$ spinel ferrite compared to the inverse spinel Fe_3O_4 NPs synthesized similarly. As a consequence, an increase in *D* was noted for magnetite relative to Mn ferrite. Such behavior can be rationalized by taking into account the larger content of highly reactive Fe(III) species in octahedral coordination in the normal ferrite. The same procedure has been used for including GO in the reaction mixture [81]; since polyols can act as reducing agents under these conditions, the simultaneous reduction of GO and the formation of ferrite NPs are verified. Other methods used for synthesizing ferrite NPs include sol-gel [28, 82, 83], micro-emulsion [10, 36, 84], biogenic [85, 86], auto-ignited combustion [87–89], electrochemical [90] and mechanical [91] methods.

4. Functionalization

Surface functionalization of nanostructured ferrites is a crucial step in the design of nanodevices for many applications since proper functionalization determines the final use and allows control over the physico-chemical processes at the surface, thus tuning several magnetic, optical and electrical properties in the desired direction. Although several synthetic methods allow in situ functionalization of obtained ferrite NPs, this approach is not always enough, and postsynthetic surface functionalization becomes necessary. For example, biomedical and environmental applications require hydrophilic NPs with definite chemical groups. The crucial feature that allows for surface functionalization is the availability of superficial transition metal *d* orbitals acting as Lewis acids in the presence of donor ligands. Fortunately, spinel ferrite surface is reactive toward many chemical groups, which provide room for multiple combinations. Ligands comprise many low and high molecular weight compounds [92]; functional groups available for surface complexation include carboxylic acids [93–95], amides [27, 29], hydroxyl [70, 96], phosphonic [73, 97] and hydroxamic acids [73].

There are mainly three approaches to make hydrophilic functional NPs: (i) ligand exchange reaction, (ii) silica coating and (iii) polymer coating. Ligand exchange reactions effectively transfer hydrophobic particles to aqueous medium by the replacement of hydrophobic ligands with hydrophilic ones, without affecting the magnetic core considerably. However, for some applications, magnetic NPs can also be transferred from polar to nonpolar mediums [98, 99]. Small ligands stabilize the NPs mainly by coulombic repulsion of ionized groups, like quaternary ammonium cations and carboxylates [100]; charged groups not only stabilize the magnetic suspension but also reinforce water affinity by facile solvation. Conversely, macromolecular

ligands stabilize NPs by interparticle steric repulsions due to extended conformations that they can adopt in contact with good solvents [101]. In cases when the polymer carries ionisable groups, as PAA [34, 93, 101], coulombic repulsions enhance their capabilities as a stabilizer.

Silica coating has the advantage that provides excellent chemical stability to the magnetic core while preventing magnetic interactions, which is traduced into colloidal stability. Following the hydrolysis-condensation method established by Stöber [102], it is possible to achieve silica shells with controlled thickness by careful addition of tetraethyl orthosilicate (TEOS) to the NP dispersion without the appearance of individual silica particles, which in turn allows for a fine-tuning of magnetic interactions [103]. Furthermore, silica coating can be functionalized with several organosilanes containing suitable groups like -SH [104–106] and -NH [105], as depicted in **Figure 2**.

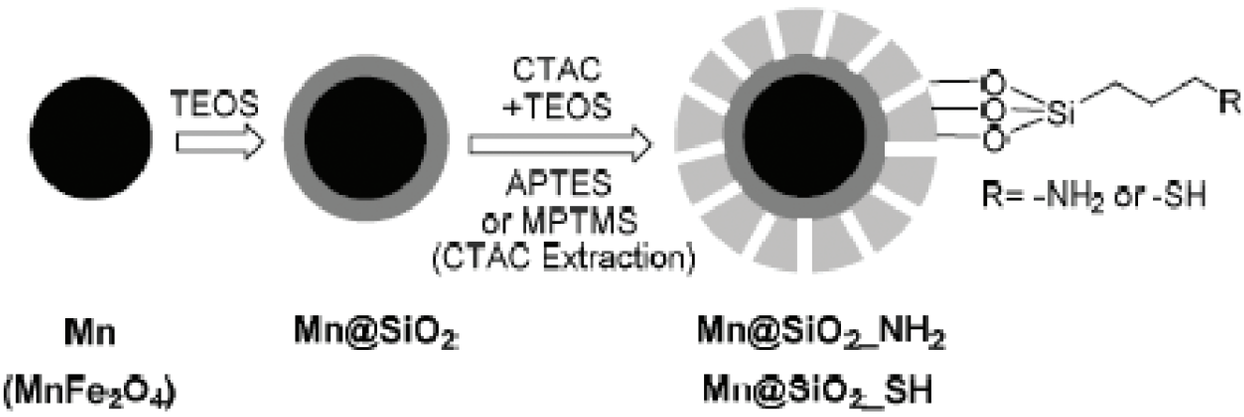

Figure 2. Scheme of the synthesis of amine and thiol functionalization of core magnetite NPs protected with a silica shell (Adapted from Ref. [105] with permission of the Royal Society of Chemistry).

Two main routes for polymer coating of NPs [107, 108] are: (i) functionalization of the NP surface with a molecule that acts as an initiator for further interfacial-controlled polymerization [109, 110] and (ii) synthesis of the polymer as the first step followed by surface anchoring [111–114]. The latter is simpler and allows for a wide variety of macromolecules, provided they bear suitable functional groups for surface binding. The former, although more laborious, has the advantage that it is possible to control the surface density of the grafted polymer and the length of the growing chains [115]. A shortcoming concerning macromolecular coating of magnetic NPs emerges when high mass magnetizations are required. Since polymers do not contribute to magnetization, mass magnetization of highly functionalized NPs drops noticeably, and so they might disable the whole system.

Conjugation after primary NP synthesis and water stabilization constitutes the final step prior to environmental and biomedical applications. It affords the ultimate precise chemical functions. Several strategies have been reported to achieve this goal entailing many known organic reactions [107]. For example, Zhao *et al.* [116] obtained hydroxamic acid-decorated Fe_3O_4/poly(acrylamide) (PAM) nanocomposites by treating the amide bonds with hydroxylamine solution and Zhao *et al.* [117] introduced amine groups by reacting ethylenediamine with a polymer containing epoxy moieties previously attached to Fe_3O_4 NPs. A very similar approach was employed in order to obtain thiol groups by adding NaSH to episulfide moieties [118]. Amide and ester formation are nice strategies to achieve NPs conjugation; in these reactions, carbodiimides are

http://dx.doi.org/10.5772/67513

used as effective coupling agents. Following this strategy, Ren *et al*. [119] incorporated EDTA ligands to Fe_3O_4@SiO_2@chitosan particles through amide bonds between EDTA $–COO^-$ moieties and $–NH_2$ groups in chitosan shell (see **Figure 3**), while Ge *et al*. [120] incorporated a polycarboxylic acid into amine-decorated magnetite. Rare sulfur-containing functional groups have been incorporated from chitosan modification, as is the case of xanthate-decorated magnetite NPs [121]. Thiol-ene reactions have also employed to include phosphonic acid moieties in a thiol-decorated nanoplatform [122]; the kinetics and efficiency of this reaction prevent phosphonic acid depletion due to surface binding. The reaction is depicted in **Figure 4**.

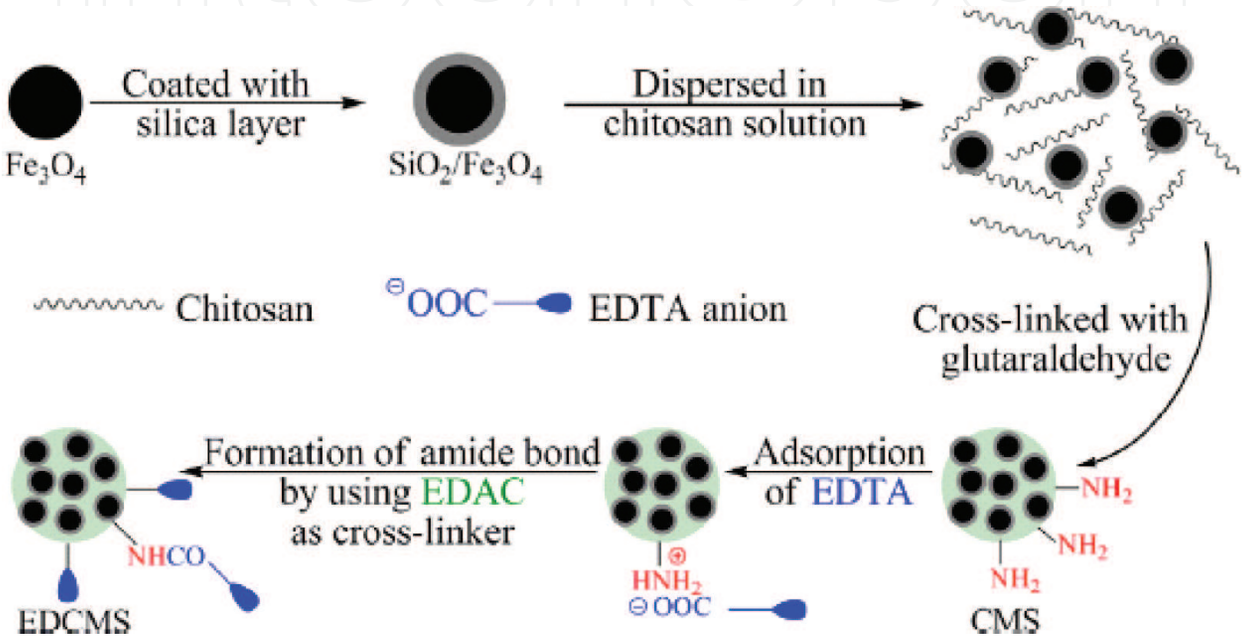

Figure 3. Synthesis of EDTA-containing magnetic NPs by amidation of chitosan (Adapted from Ref. [119] with permission of Elsevier).

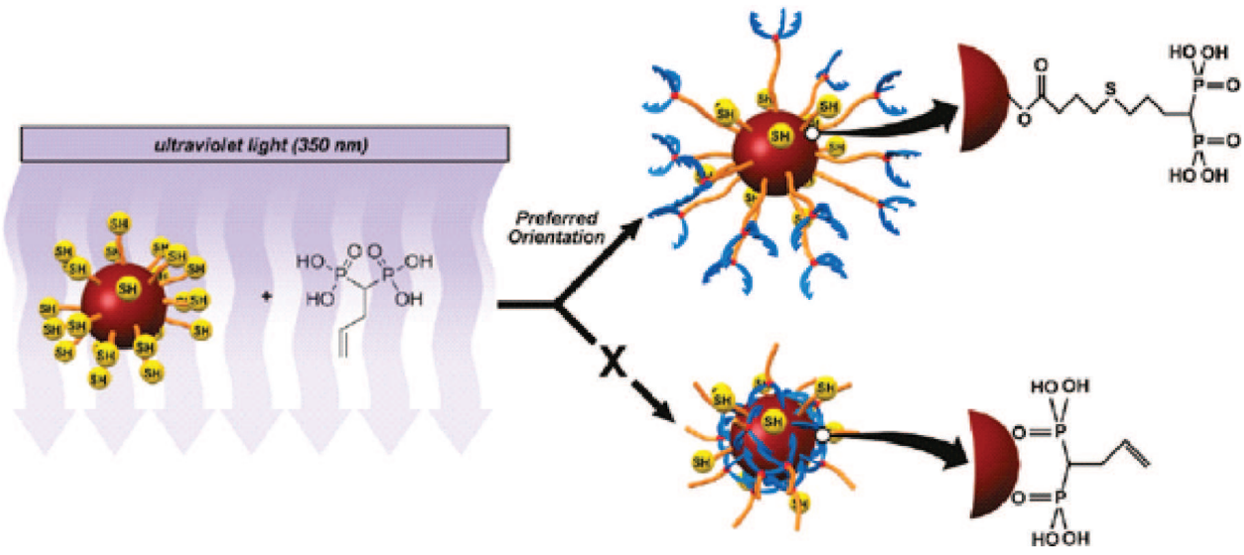

Figure 4. Synthesis of diphosphonic acid-containing magnetic NPs by a facile thiol-ene reaction (Adapted from Ref. [122] with permission of the American Chemical Society).

Coordination reactions like MOF construction have also been developed at ferrite surface. Fe_3O_4 NPs decorated with carboxyl groups were conjugated with a zeolitic imidazolate framework (ZIF-8) for the adsorption of contaminants [123, 124]. Such MOF was grown in a step-by-step assembly, initiated by the Zn^{2+} chelation to the oxide surface through carboxyl groups, resulting in a magnetic core surrounded by the ZIF shell. By varying the number of growth cycles, it is possible to tune the thickness of the MOF shell and hence, the interparticle distance between the magnetic cores. Another inorganic reaction at the interface of magnetic NPs reported recently [125] consists of the deposition of hydrous lanthanum oxide over Fe_3O_4@SiO_2

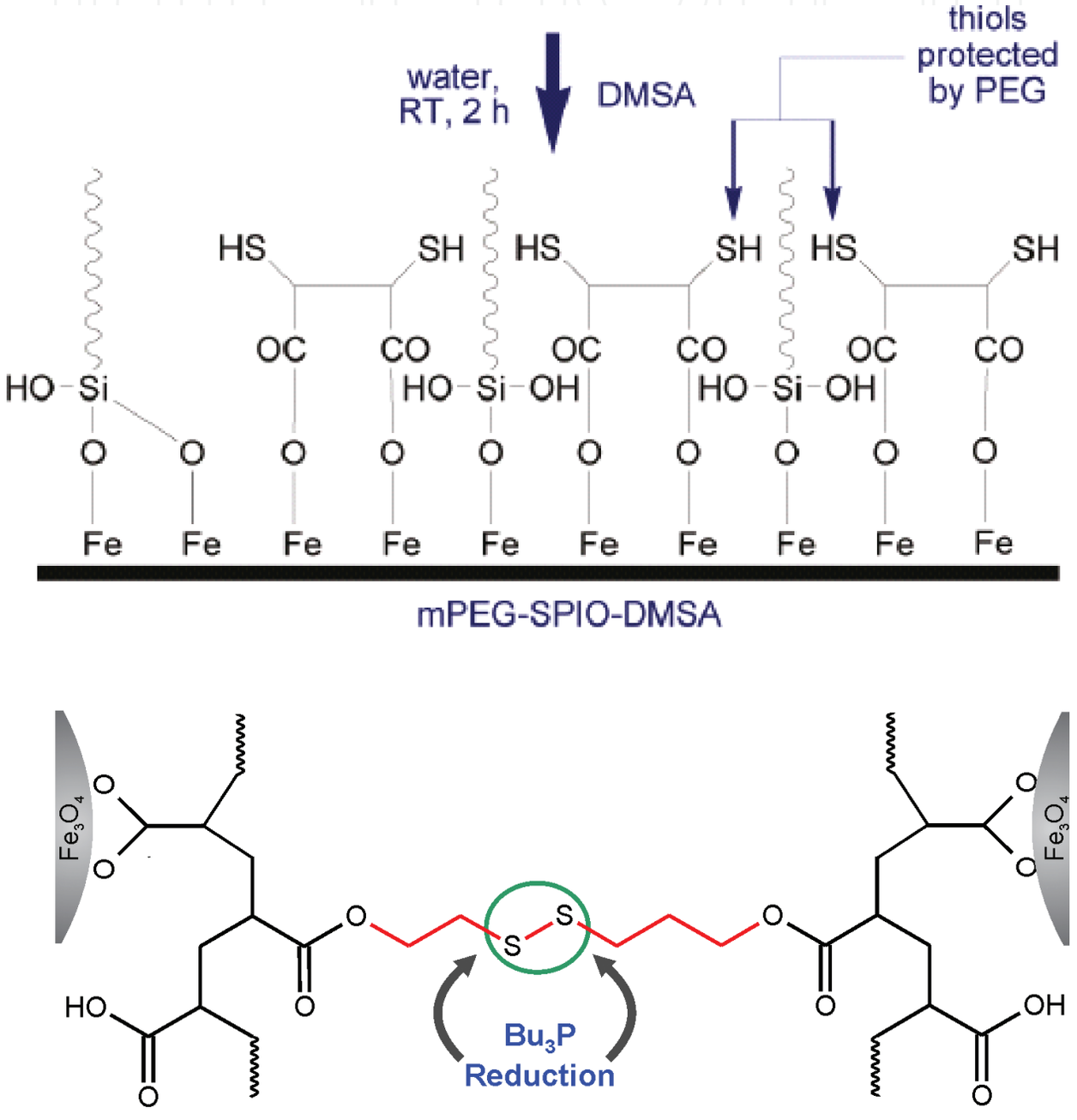

Figure 5. Two methods for thiol protection. *Top:* Steric hindrance by surface PEG grafting (Adapted from Ref. [130] with permission of the American Chemical Society). *Bottom:* Reversible thiol oxidation to disulfide bridges (Reproduced from Ref. [34] with permission of Elsevier).

http://dx.doi.org/10.5772/67513

core-shell NPs simply by adding $LaCl_3$ at basic pH in the presence of the magnetic material. Nanostructures composed of ferrites and noble metals have interesting and promising optical and magnetic properties; the synthesis of such materials can be easily performed by reduction of the corresponding metal salt in the presence of ferrite NPs [126].

In the case of surface thiol-decorated nanostructures, special care must be taken, since free thiol groups are prone to be oxidized during the synthetic procedures. For example, several papers have reported the oxidation of DMSA and cysteine to disulfide and sulfoxide compounds in the presence of Fe_3O_4 NPs [24, 127–129]; these undesirable processes not only reduce the effective amount of –SH groups but also could alter magnetite phase. To overcome this drawback, Maurizi *et al.* [130] grafted PEG chains onto the oxide surface as steric barriers in order to avoid the formation of intermolecular disulfide bridges between adjacent DMSA molecules. More recently, Odio *et al.* [34] designed a novel PAA copolymer containing disulfide bridges; after Fe_3O_4 functionalization with this polymer, resulting NPs were treated with tributyl phosphine in order to reduce disulfide bridges to free –SH groups. Both strategies are depicted in **Figure 5**.

5. Coordination chemistry at the surface

Since the nature of the metal-ligand interactions at the interface of the ferrites plays a key role in the properties of NPs, efforts have been devoted to unravel the structure and implications of the surface complexes occurring for different types of ligands. For this purpose, spectroscopic techniques like FTIR, XPS, EXAF and XANES are usually employed [22, 24, 58, 122, 131–133]. Mössbauer spectroscopy has also been used since iron spectra are sensitive to spin reorganization after ligand binding and to the kind of iron site that participates in the surface complexes [23, 58, 131].

Specifically, Daou *et al.* [131] showed that phosphate ligands bind to magnetite surface by forming bidentate binuclear complexes with octahedral Fe(III) cations. In contrast, Costo *et al.* [21] suggested that phosphonates bind to the surface through mono-dentate ligands. For carboxylates, it is reported that in solvothermal and thermal decomposition methods, OA is anchored to the surface by bridging bidentate complexes [22, 24, 134], a conclusion supported by a theoretical DFT study showing that the bidentate mode was the most stable configuration of iron-oleate complex no matter the surface plane exposed to the ligand [135]. However, after ligand exchange reactions with other carboxylic acids, carboxylate complexes could form chelates [24, 34, 136]. The use of amine functional groups showed that long-chain amine molecules adsorb at the surface of ferrites by N-metal interactions [16, 137]. In contrast, if both OA and OAm are used in the ferrite synthesis, the mode of coordination of each functional group could depend on the concentration and molar ratio of the surfactants. Thus, if the surfactants are diluted in N-methyl 2-pyrrolidone with a molar ratio 1:1, Verma and Pravarthana [58] suggested by means of IR analysis that OA complexes retain the bidentate mode while OAm molecules appear protonated and associated to the surface through coulombic interactions. However, XPS studies of Wilson and Langell [133] indicated that if the reaction is performed without a solvent and a higher OAm proportion is employed, OAm is

anchored to the surface by Fe-N coordination, while OA binds to the surface though a monodentate complex. Using IR studies, alcohols are reported to be anchored to the oxide surface by metal-OH interactions [70]. Besides, ligands with thiol moieties anchor to magnetite surface by Fe(II)-S interactions, as suggested by IR and XPS studies [24, 138]. Finally, cyclic amides like PVP and 2-pyrrolidone seem to interact with ferrite surfaces through the carbonyl groups [27, 29]. Since this subject is not yet completely understood, computational methods are likely necessary to unravel the structural and electronic properties of surface complexes.

6. Environmental applications

In this section, we focus on two applications of nanostructured spinel ferrites for environmental remediation technologies in connection with water decontamination: adsorption and oxidation technologies.

6.1. Adsorption technologies for removal of inorganic and organic contaminants

Adsorption is often the most suitable choice for removal of toxic substances in drinking or waste waters, mainly due to its simplicity and high efficiency; the main disadvantage is the sorbent separation after the adsorption process, which can become tedious and energy consuming. However, the use of magnetic materials for adsorption makes the task of sorbent separation easier by allowing magnetic decantation with a permanent magnet. The high surface area of ferrite NPs along with their room temperature superparamagnetism and the great versatility for binding specific functional groups on their surfaces for specific contaminants makes them ideal candidates for the design and development of innovative adsorption strategies. Although several recent reviews covering this subject are available [6, 7, 139, 140], these have generally focused on the thermodynamics and kinetics of the adsorption process and relatively less attention has been paid to unravel the atomic and molecular nature of the interactions occurring at the interface. Although this is a difficult task, this information is crucial for the improvement and optimization of the nanoadsorbent.

6.1.1. Heavy metal cations

Heavy metal cations, found in natural and waste waters resulting from industrial activities, comprise a wide family of hazardous substances with a high impact on human health [141]. Here, we concentrate on those reported studies with a focus on two directions: (i) improving the adsorption capacity and/or selectivity toward a given contaminant by surface functionalization of ferrite NPs and (ii) shedding light on the adsorption mechanism at a molecular and atomic level.

6.1.1.1. Amine-functionalized nanosystems

Fe_3O_4 NPs functionalized with several amino-containing polymers were tested as Cr(VI) and Cu(II) sorbents in aqueous medium [142], showing the increase of adsorption capacity for both cations with the number of –NH moieties in the ligand incorporated to the magnetic nanoplatform. Adsorption and spectroscopic data suggested that metal removal involves

coulombic interactions, ion exchange processes and formation of complexes between amine groups and metal ions, although the structure of such complexes was not revealed. Similar results were reported by Huang and Chen [113], in which Fe_3O_4@PAA NPs decorated with amine groups were proved as a good adsorbent for several heavy metals with positive and negative charges; based on pH studies, authors suggested that cations are adsorbed through chelate complexes while anions are incorporated after ion exchange mechanisms. New insights about Cr(VI) adsorption with an amino-decorated magnetic sorbent were reported by Zhao *et al.* [143]. This approach comprises nanocomposites of Fe_3O_4 and amino-functionalized GO sheets. Based on XPS measurements, authors suggested that after attractive coulombic interactions between chromate species and protonated amino groups, a fraction of Cr(VI) is reduced to Cr(III), which further forms amino-complexes; the source of electron for Cr(VI) reduction is provided by the GO sheets. Without extra evidence, these results should be taken with care because XPS deconvolution was not rigorous.

Amino-functionalized Fe_3O_4 NPs were tested as a sorbent for Cu(II), Cd(II) and Pb(II) [144]. Adsorption decreased at acid pH values and adsorption capacity for Cu(II) was higher than that for softer Lewis acids Cd(II) and Pb(II). Both results, along with thermodynamic and kinetic data, could indicate the prevalence of coulombic and complexing reactions between surface –NH moieties and the cations. Similar results were presented in other reports [52, 145]. Co-ferrite NPs coated with a polystyrene shell modified with amino and thioether groups were tested for Hg(II) adsorption [146]. Authors proposed the Hg(II) complexation by these functional groups, followed by partial reduction of Hg(II) to Hg(I), although no proof for this mechanism was presented.

6.1.1.2. Carboxyl-functionalized nanosystems

Several reports have focused on the adsorption of heavy metal cations by EDTA-modified magnetic nanosystems in order to take advantage of the high chelating ability of this multifunctional ligand. The key role of EDTA has been confirmed since the adsorption capacity decreases when no EDTA was used in the preparation of the sorbents. Indeed, Ren *et al.* [119] noted that the adsorption capacity follows the same order of the metal-EDTA complex stability: Cu(II) > Pb(II) > Cd(II). Similar conclusions are drawn from recent reports [147, 148] in which the formation of metal-carboxylates was verified by means of FTIR measurements. Carboxyl-decorated NPs from acrylic and crotonic acid copolymer were tested for Cu(II), Pb(II), Zn(II) and Cd(II) [120]. Although authors did not show spectroscopic evidences of metal-carboxylates interactions, the maximum adsorption capacity increases with the increase in Lewis acid hardness of the ion tested (Cu(II) > Zn(II) ≈ Pb(II) > Cd(II)). Likewise, Mahdavian *et al.* [149] studied the adsorption behavior of Pb(II), Cu(II), Ni(II) and Cd(II) with a nanoplatform consisting of PAA chains grown at the surface of magnetite NPs and found that the metal uptake increases with pH, suggesting chelate formation. Other carboxyl-based magnetite NPs for Pb(II) removal can be found elsewhere [150].

6.1.1.3. Thiol and other sulfur-containing compounds functionalized nanosystems

Fe_3O_4 NPs functionalized with a polythiolated ligand was probed as Hg(II) adsorbent [118]. XPS studies supported the occurrence of Hg(II)-S interactions and the simultaneous reduction

of Hg(II) to Hg(I) likely at the expense of Fe(II) cations at the surface of the magnetic core. Curiously, no sign of thiol oxidation was encountered. Recently, Wang *et al.* [151] tested a simpler Fe_3O_4@SiO_2-RSH nanoplatform toward Hg(II), Pb(II) and Cd(II) ions. Although no mechanism was elucidated, the fact that the adsorption capacities followed the order Hg(II) >> Cd(II) > Pb(II) might be indicative of two phenomena: (i) metal uptake is governed by soft-soft interactions between the cations and the thiolate groups and (ii) for the case of Hg(II) ions, adsorption involves reduction. A similar $CoFe_2O_4$@SiO_2-RSH nanosystem for Pb(II) removal has been employed, but no mechanism was proposed [152].

Zhu *et al.* [121] designed a Fe_3O_4/chitosan-OC(=S)SH platform for Pb(II), Cu(II) and Zn(II) adsorption. FTIR and XPS suggested that metal-ligand interactions comprise both the N atom of the residual chitosan amine groups and the sulfur groups of xanthate moieties. However, neither the specific role of each functional group nor the structure of such complexes was elucidated. Based on the adsorption capacity order Cu(II) >> Pb(II) ≈ Zn(II), it is likely that relative hard chitosan N groups play an important role in the overall performance of the adsorbent. Alternatively, Zhang et al. [72] chose nanocomposites of Fe_3O_4 and thiolated CNTs as sorbents for Pb(II) and Hg(II) ions. Thiol grafting material proved to be a better adsorbent than Fe_3O_4/CNT composites. Adsorption capacity is larger for softer Lewis acid Hg(II), which could imply the occurrence of metal-thiol complexes. A similar trend was found in another report [106].

Fe_3O_4 NPs functionalized with a copolymer obtained by the partial modification of PAA with thio-salicyl-hydrazide were tested for several divalent cations [153]. This system contains both soft (thiol) and hard (carboxyl and amine) moieties, which might explain the good adsorption properties toward soft Cd(II) and hard Co(II) cations. Regarding Pb(II) uptake, XPS studies confirmed the presence of Pb-S interactions; it is interesting that only one contribution was proposed for the deconvolution of the Pb 4f spectrum, which implies that there is only one coordination environment for Pb(II) cations. The prevalence of Pb-S interactions is coherent with the small interference effect produced by alkaline/earth metals, since these hard cations largely prefer hard ligands.

Surface ion imprinting techniques can also be used for efficient and selective sequestration of heavy metal cations. Guo *et al.* [154] added Fe_3O_4@SiO_2 NPs to a solution containing the Pb-MPTS complex as a template. Condensation of silane groups followed by Pb(II) removal with HCl results in imprinted cavities with the proper thiol configuration (**Figure 6**). This nanosystem was shown to be a good adsorbent toward Pb(II) ions with excellent selectivity over other heavy metals like Cu(II), Zn(II) and Co(II). In this case, selectivity is not only ruled by the chemical affinity between cation and thiols but it also depends on the ionic radius, coordination number and coordination geometry.

Yantasee *et al.* [155] employed Fe_3O_4@DMSA NPs for the removal of several cations, suggesting that metal adsorption was driven by free –SH groups, while –COOH groups were anchored to the magnetic core. However, no evidence regarding either the state of the sulfur before and after metal incorporation or the nature of metal-S complex was presented. Afterward, Odio *et al.* [24] tested the adsorption capabilities of the same nanoplatform aiming at Au (III). By means of XPS and UV-vis analysis, they found that before adsorption, DMSA ligands

http://dx.doi.org/10.5772/67513

are mostly oxidized to disulfide bridges and Au(III) could adsorb onto Fe_3O_4@DMSA NPs by three possible ways: (i) chelation with free –COOH moieties; (ii) reduction to Au^0 sub-nanometer clusters triggered by surface Fe(II) oxidation in the bare sectors of the NPs and (iii) extensive reduction to Au^0 nanoclusters in the region covered by the organic ligand, which is caused likely due to oxidation of disulfide bridges to –SOx species. The process is depicted in the upper part of **Figure 7**. On the contrary, when Pb(II) was tested with the same material, the results indicated that neither Pb reduction nor Pb-S interactions contribute to the adsorption process, but it is solely caused by the occurrence of chelating carboxylates and oxo-complex at bare sectors [34]. In order to unravel the actual role of both –SH and –COOH functions in the adsorption of hardly reducible divalent cations, the same group studied the adsorption of Pb (II) and Cd(II) by a novel nanoplatform based on Fe_3O_4 NPs capped with a copolymer with pendant free –COOH and –SH groups [34]; thiol moieties were protected during the synthesis to avoid oxidation and were regenerated just before the adsorption experiments. A detailed XPS analysis indicated that both metal-carboxylate and metal-thiolate interactions are verified during adsorption. In addition, it was shown that although both cations showed higher affinity to thiols, this tendency was more pronounced for Cd(II), that is, Pb(II) is less selective, in agreement with its borderline softness characteristics. Nevertheless, the actual structure of the surface metal complexes is still elusive.

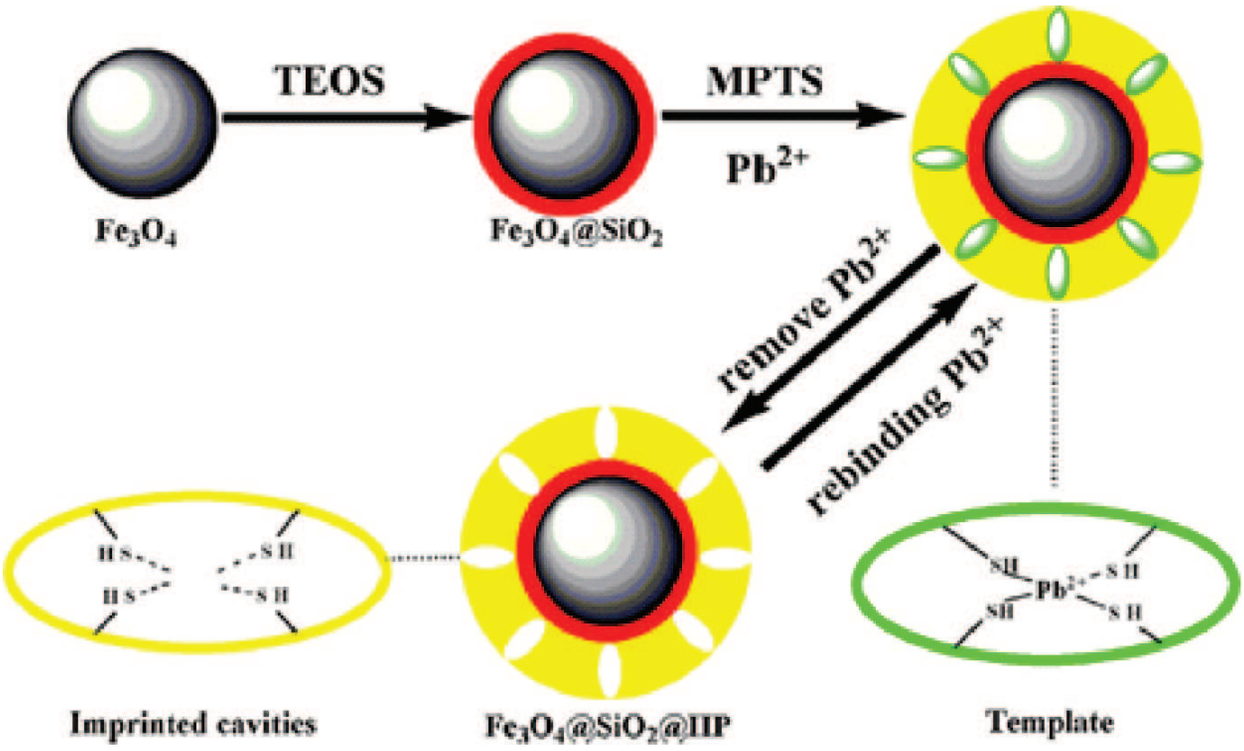

Figure 6. Surface ion imprinting technique for selective adsorption of Pb(II) ions onto magnetic NPs (Adapted from Ref. [154] with permission of Elsevier).

6.1.1.4. Other functional groups and particles with a bare surface

Fe_3O_4/PAM nanocomposites functionalized with hydroxamic acid moieties were shown to adsorb Pb(II), Cd(II), Co(II) and Ni(II) ions by forming bidentate chelating complexes [116].

The key role of hydroxamic groups was demonstrated, which agrees with the fact that the stability constant of metal-hydroxamic complexes follows the same order as the maximum adsorption capacity. The structure of these surface complexes was determined from IR and DFT studies and the system was selective toward Pb(II) uptake.

Rutledge *et al.* [122] designed a nanoplatform decorated with diphosphonic acid and thiol moieties for Pb(II), Hg(II) and f-block elements like La(III) and Eu(III) adsorption. Comparison between different adsorption sites suggested that both hard Lewis acid cations La(III) and Eu (III) are efficiently adsorbed by a hard Lewis base as diphosphonate groups, but they are inert toward thiol-mediated binding, in accordance with the soft nature of this Lewis base. However, Hg(II) uptake showed the inverse tendency, being very sensitive to –SH moieties, but a kind of unreactive toward diphosphonate basic functions. On the contrary, Pb(II) did not display such selectivity toward a particular functional group, but it showed a synergic effect upon ion uptake. The same behavior for Pb(II) was mentioned above: the fact that Pb(II) cation

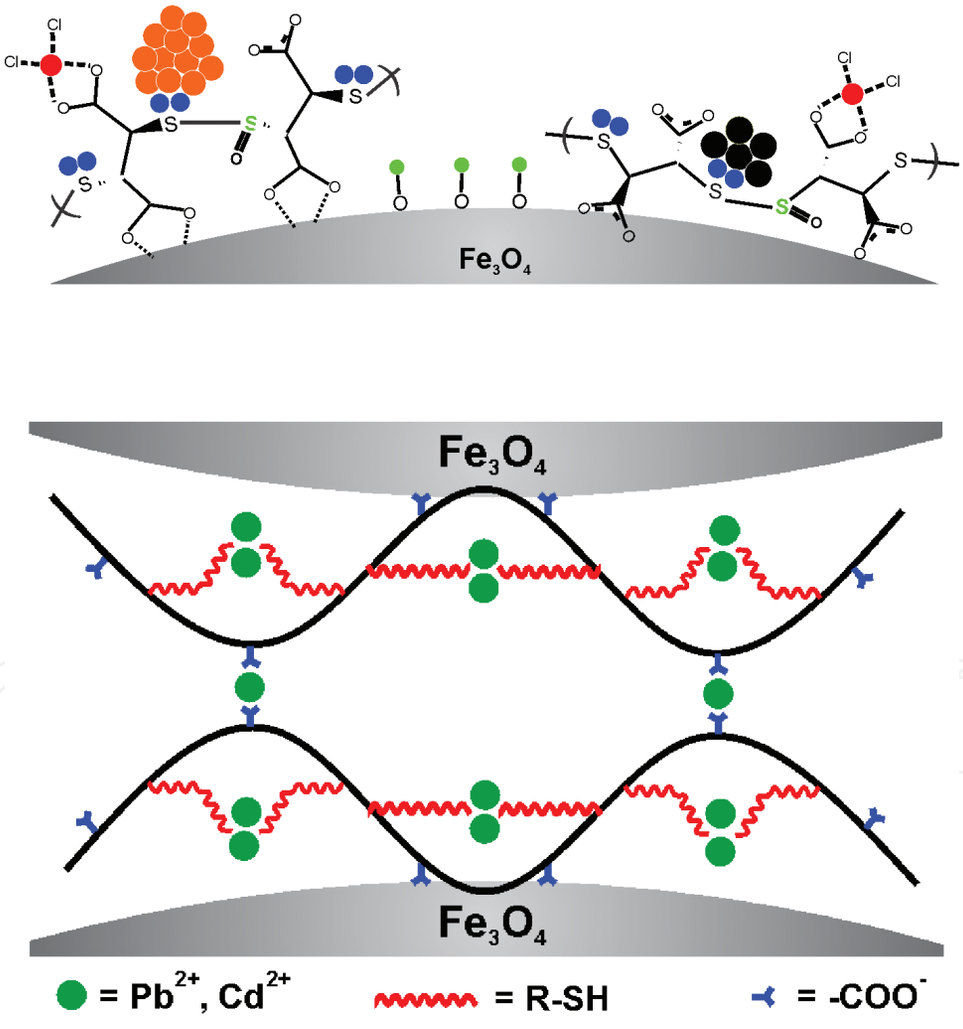

Figure 7. *Top:* Likely distribution of Au atoms during adsorption onto Fe_3O_4@DMSA NPs; different colors correspond to distinctive Au 4f XPS signals. *Bottom:* Likely distribution of Pb(II) and Cd(II) cations during adsorption onto the thiol- and carboxyl-containing Fe_3O_4 NPs; note the preponderance of metal-thiol interactions over metal-carboxylate ones (Adapted from Ref. [34] with permission of Elsevier).

can bind a wide variety of hard and soft ligands is related with unique electronic properties steaming from relativistic effects [156]. Further theoretical and experimental investigations on this issue are still needed.

Given that surface magnetite NPs biosynthesized by microorganisms are richer in Fe(II) content with respect to stoichiometric Fe_3O_4, this biomaterial has been tested for the adsorption and reduction of toxic oxyanions containing Cr(VI) and $m^{99}Tc$(VII) [85]. Results confirm that biomagnetite is a better absorber compared to a commercial magnetite of similar size, and the removal capacity changes with the particular iron substrate that was used for bacteria culture. The adsorption-reduction mechanism of chromate anions was studied by means of XPS and X-ray magnetic circular dichroism (XMCD). Authors suggested that after the fast electron transfer reactions between Cr(VI) and surface Fe(II), Cr(III) ions are incorporated into the spinel structure and occupy octahedral interstices, thus forming a layer of ferrimagnetic $CrFe_2O_4$ spinel.

6.1.2. Arsenic, phosphorous and fluoride

In a careful spectroscopic study, Liu *et al.* [157] studied As(V) and As(III) adsorption onto 34 nm magnetite NPs, avoiding the presence of oxygen during the adsorption procedure. After EXAF and XANES analysis, they confirmed that arsenate is adsorbed as a bidentate binuclear corner-sharing complex, while arsenite binds to the surface through a tridentate hexanuclear corner-sharing complex (see the left panel of **Figure 8**). Also important, they noted, based on XPS analysis, that if anoxic conditions are fulfilled, no redox reactions involving arsenic species are verified. This result disagrees with other reports [158, 159] that claimed for redox reactions

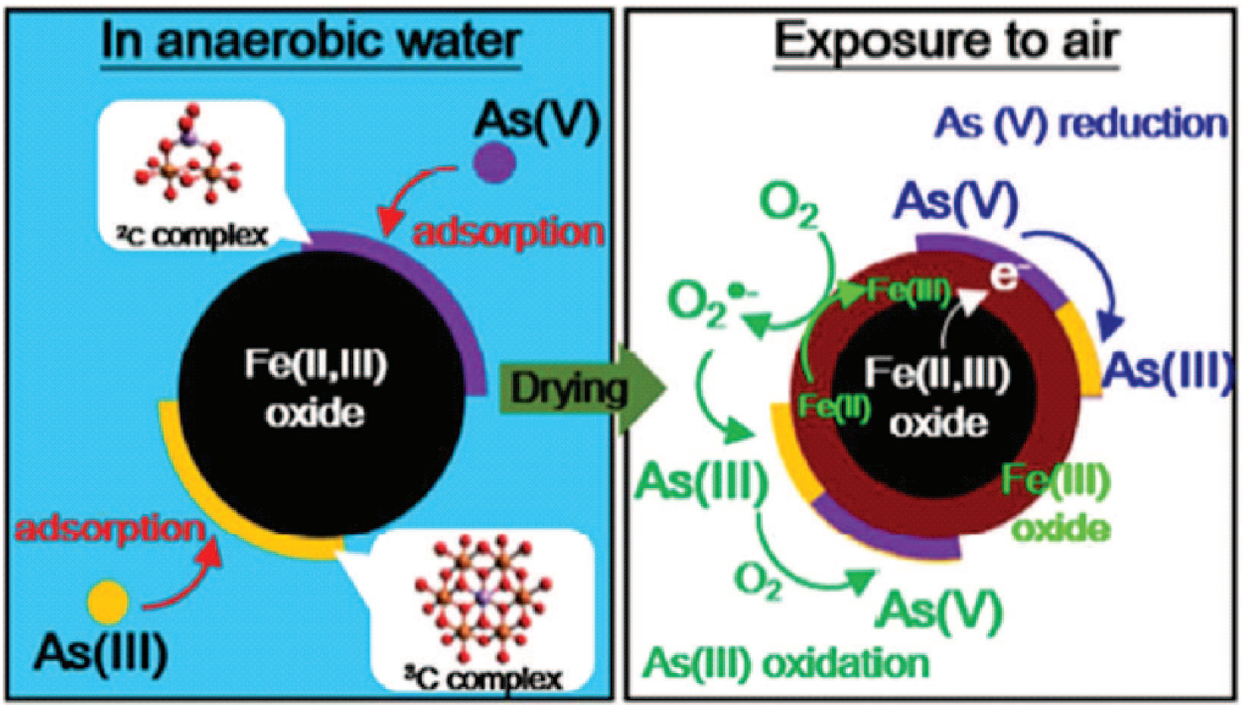

Figure 8. *Left:* Geometry of surface complexes during As(V) and As(III) adsorption onto magnetite surface in anaerobic aqueous medium. *Right:* possible redox reactions occurring at the As-Fe_3O_4 interface when exposed to air (Reproduced from Ref. [157] with permission of the American Chemical Society).

during adsorption and generates a reasonable doubt about the role of the magnetite surface in the arsenic redox processes. On the contrary, after exposure of the adsorbed material to aerobic conditions, XPS analysis showed substantial amounts of As(V) in the As(III)-treated NPs and As (III) in the As(V)-treated NPs. In both samples, the Fe(II)/Fe(III) molar ratio was less than 0.5, denoting Fe_3O_4 oxidation to γ-Fe_2O_3. As(III) oxidation to As(V) can be caused by oxygen contact. On the other hand, As(V) reduction to As(III) was explained assuming that during magnetite oxidation, an electron flow from the core to the surface takes place; eventually, these electrons could cause As(V) reduction. Both processes are depicted in the right panel of **Figure 8**.

Zhang *et al.* [160] employed Fe_3O_4/activated carbon fiber nanocomposites for As(V) removal. Based on XPS studies, authors claimed the occurrence of inner-sphere bidentate complexes between the mono-protonated anion and surface oxygen anions from either the magnetite phase or the carbon fibers. In contrast, no redox reactions were claimed. Another carbonaceous material in conjunction with ferrites has also been tested for arsenic removal. Lingamdinne *et al.* [55] chose 30 nm porous $NiFe_2O_4$/rGO nanocomposites and concluded that the high removal efficiency is due to the extended porous structure of the composite, which favors adsorption. The authors claimed that adsorption involves both electrostatic attraction and surface-complexation reactions, but to our understanding, this issue was not totally clarified.

Another recent report uses Fe_3O_4@ZIF-8 as a sorbent [123]. In this case, arsenic adsorption is entirely caused by the ZIF-8 shell, while magnetite core only acts as a magnetic device to remove the contaminant in a facile and efficient way. Alternatively, magnetite particles encapsulated with calcium alginate were tested as an adsorbent for inorganic and organic As(V) species [159]. The authors found that inorganic species are better adsorbed than monomethyl arsenate. Based on IR and XPS measurements, they suggested that arsenic incorporation likely occurs through the partial reduction of As(V) to As(III) species and the oxidation of both alginate and magnetite. However, spectroscopic studies were not conclusive.

A recent report from Penke *et al.* [161] deals with As(III) and As(V) adsorption onto 20–30 nm Al-substituted $NiFe_2O_4$ NPs. Based on Raman, FTIR and XPS studies, the authors proposed that both species are adsorbed onto the ternary oxide surface through inner-sphere complexes. In addition, redox reactions between the spinel and arsenic species were claimed. However, this report does not clarify either the geometry of the formed surface complexes or the nature of the implicated redox reactions, although it showed that the replacement of Fe(III) cations by Al(III) cations enhances the adsorption properties of the oxide due to an increase in the number of surface hydroxyl groups. Similar conclusions were drawn from the work of Peng *et al.* [162]. In this case, Fe_3O_4@$Cu(OH)_2$ core-shell nanostructures were tested as adsorbents for As(V). They stressed the key role of surface hydroxyl groups of the copper shell and suggested that arsenate complexes are formed at the surface. However, the proposed complex structure is not rigorously justified.

The use of metal hydroxides can be extended to other elements of group V like phosphorus. Thus, Lai *et al.* [125] employed a shell of hydrous lanthanum oxide incorporated into Fe_3O_4@SiO_2 NPs to drive the removal of phosphate anions from the water medium. The adsorption was fast and efficient given the high affinity of La(III) species toward phosphate ligands. This methodology overcomes the use of bare Fe_3O_4. Fe_3O_4/polypyrrole nanocomposites were employed for

removing fluoride anions without interference effects [163]. Based on thermodynamic and kinetic data, authors postulated an ion exchange mechanism.

6.1.3. Dyes

Extensive use of organic dyes has become a serious environmental problem since this family of organic compounds is difficult to decompose and transforms to carcinogenic amines. A series of ferrite MFe_2O_4/rGO ($M = Mn^{2+}$, Ni^{2+}, Zn^{2+}, Co^{2+}) nanocomposites were tested as combined magnetic materials for adsorption and photocatalytic degradation of Methylene Blue (MB) and Rhodamine B (RhB) under visible light [81] (see Section 6.2). Authors devoted the high adsorption capacity and fast removal rate to the large surface area of the material. For this system, though electrostatic interactions cannot be ruled out, dye retention is mainly caused by the rGO sheets, comprising π-π stacking interactions between the aromatic moieties of the dyes and the extended π-conjugated regions in the graphene structure. The same mechanism was claimed earlier using Fe_3O_4/rGO nanocomposites for MB adsorption [164]; this report also tested other materials like activated carbon and multi-walled carbon nanotubes (MWCN).

Cobalt ferrites covered by PEG chains were shown to be good adsorbents for several dyes such as methyl orange (MO), MB and Congo red (CR) [75]. Adsorption data indicate that electrostatic interactions are not the prominent cause for adsorption; instead, H-bonding interactions between –OH groups of PEG and functional groups in the dyes seem to be the responsible cause. The interactions are depicted in **Figure 9**. H-bonding has also been claimed as the main interaction of several dyes with naked $MnFe_2O_4$ NPs [43].

In a recent work, Dolatkhah and Wilson [114] functionalized Fe_3O_4 NPs with chitosan grafted with PAA and poly(itaconic) acid (PIA) chains. This polymeric material displays reversible pH-responsive behavior, which was tested for MB adsorption. As the pH increases, the ionization of the chitosan-grafted acid groups also increases, favoring the expansion of the grafted chains and the ionic interactions with MB, since this dye is cationic. Hence, adsorption is favored. Afterward, the desorption of MB is accomplished simply by acidification until dye-sorbent interactions become very weak and the polymeric chains no longer stabilize the colloid, leading to the collapse of the dye-free NPs. The process is represented in **Figure 10**.

6.1.4. Aromatic compounds and other organic pollutants

Rodovalho *et al.* [98] employed mixed Mn and Co ferrite functionalized with carboxyl-terminated polydimethylsiloxane brushes for the adsorption of toluene in water. Significant hydrophobic interactions between toluene and polymeric chains lead to high adsorption capacity of the NPs. Moreover, authors exploited the suitable magnetic characteristic of this mixed ferrite for fast and efficient toluene desorption through hyperthermia treatment of the toluene-loaded nanoadsorbent. McCormick and Adriaens [86] employed ultra-small biogenic magnetite in the reductive transformation of CCl_4, stressing the key role of octahedral Fe(II) cations and the importance of the electron hopping between Fe(II) and Fe(III) cations in the **B** sites, which enables a good electron mobility for the surface reduction of CCl_4. Efficient adsorption of tetracycline and diclofenac by proper functionalization of magnetic nanostructures has also been reported [165, 166].

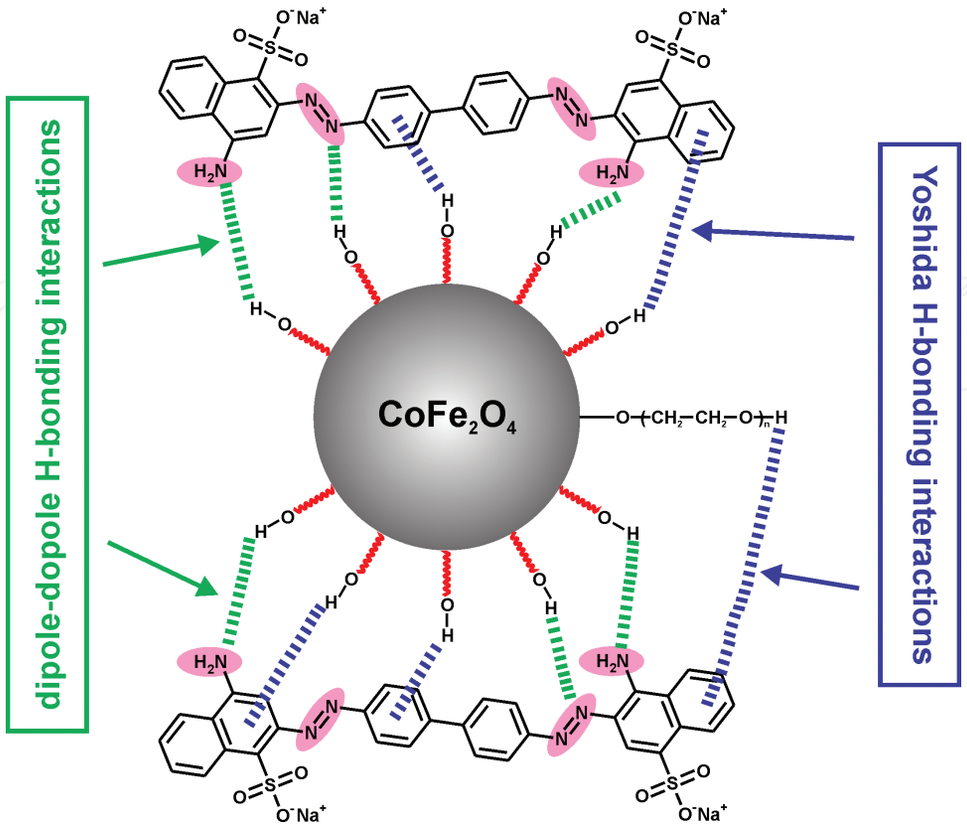

Figure 9. Proposed mechanism for CR adsorption onto PEG-functionalized MFe_2O_4 NPs (Adapted from Ref. [75] with permission of Elsevier).

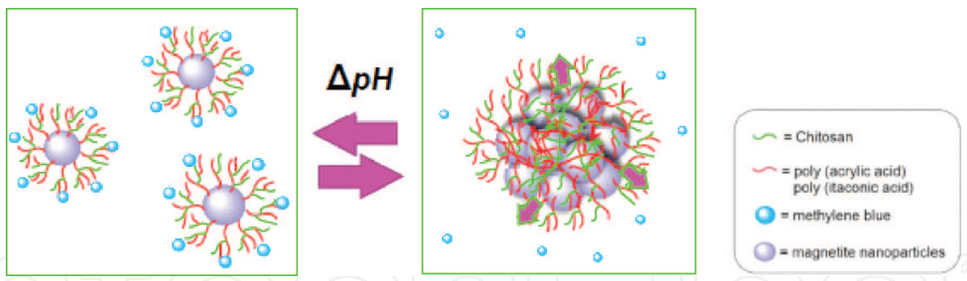

Figure 10. Mechanism of reversible pH-responsive behavior (Adapted from Ref. [114] with permission of the American Chemical Society).

6.2. Advanced oxidation technology

Advanced oxidation technologies consist of the assisted degradation of a given pollutant by using a source of highly oxidizing transient species. Such species are generally activated by the action of another substance that acts as a catalyst. Since the removal, reuse and toxicity of catalysts are major concerns, investigations have focused on the development of heterogeneous magnetic materials that can activate efficiently the oxidative degradation of the pollutants and at the same time minimize secondary contamination events. Taking into account these requirements, it is not surprising that the growing interest in ferrite NPs is due to the

http://dx.doi.org/10.5772/67513

following reasons: (i) large surface area enhances the catalytic activity; (ii) the onset of superparamagnetism enables facile removal of the catalyst; (iii) versatility of ferrite compositions makes feasible the tuning of the optical band gap of the material enabling photo-degradation approaches and (iv) chemical stability of the ferrite structure avoids metal leaking to the environment.

Nanostructured $CoFe_2O_4$ is shown to be a promising material for heterogeneous peroximonosulfate (HSO_5^-) activation in order to generate sulfate radicals ($SO_4^{-\bullet}$) that promote the oxidative decomposition of organic pollutants like 2,4-dichlorophenol [167]. The convenience of this ferrite over other cobalt oxides stems from the fact that Fe(III) cations easily cause the hydrolysis of water, leading to surface Fe(III)-OH species that can be further converted into surface Co(II)-OH complexes. In turn, such complexes are the key for the reaction of HSO_5^- to yield the $SO_4^{-\bullet}$ radicals that promote pollutant decomposition. Besides, $CoFe_2O_4$ NPs present other advantages such as no Co(II) leaching and suitable magnetic properties for the easy recovery of the catalyst. $CuFe_2O_4$ NPs have also been employed for the HSO_5^- activation in the catalytic degradation of atrazine [168] and tetrabromobisphenol [82]. In both cases, the HSO_5^- decomposition was claimed to be triggered by the cycle Cu^{2+}/Cu^{+} [168]. This is in disagreement with the report of Zhang *et al*. [169], which assigned the main role to the redox pair Cu^{2+}/Cu^{3+}. Other oxidation technologies with the aid of ferrite NPs entail the persulfate ($S_2O_8^{2-}$) [170] and H_2O_2 [12, 44, 81] heterogeneous activation for the decomposition of a wide range of organic pollutants.

An improvement in the catalytic properties of ferrites can be assessed by using composites with rGO [53, 54, 81] and MWCNs [83]. Such a synergic effect is attributed to the large surface area of the composites and to the electronic properties of these carbon-based functional materials. The proposed mechanism is outlined below [171]. It comprises the initial formation of the electron-hole pair in the ferrite phase by photon absorption (I), followed by the rapid electron transfer reaction from the ferrite conduction band to the rGO sheets (II). H_2O_2 is then decomposed in the vicinity of the rGO producing highly oxidative •OH radicals (III), which are also formed from the remaining holes in the ferrite (IV). As can be seen, step (II) is crucial for the efficient separation of photo-generated carriers, which is facilitated by the high electron conductivity of the conjugated π structure of the rGO sheets, which inhibits electron-hole recombination [172]. Moreover, •OH radicals are generated close to the rGO-adsorbed target organic pollutants, thus enhancing the decomposition rate.

$$MFe_2O_4 + h\nu \rightarrow MFe_2O_4\ (h + e) \quad \text{(I)}$$

$$MFe_2O_4\ (e) + rGO \rightarrow MFe_2O_4 + rGO\ (e) \quad \text{(II)}$$

$$rGO\ (e) + H_2O_2 \rightarrow rGO + {\bullet}OH + OH^- \quad \text{(III)}$$

$$MFe_2O_4\ (h) + OH^- \rightarrow MFe_2O_4 + {\bullet}OH \quad \text{(IV)}$$

Along the same lines, Fu *et al.* [172] noted that in the case of $CoFe_2O_4$/rGO nanocomposites with 40% of GO, there is no need for H_2O_2 to achieve efficient catalytic degradation of several dyes. Other materials for dye degradation involving ferrites are $CoFe_2O_4/TiO_2$ nanocomposites [173].

7. Concluding remarks and perspectives

- Synthesis techniques for nanostructured spinel ferrites are available to tune their magnetic properties.
- The nanoparticle surface is able to bind a wide variety of molecules with distinct functional groups that not only contribute to colloidal stabilization but also serve as the starting point for further conjugation steps. Many organic and inorganic reactions can be driven at the surface of ferrites, which allow for the tailoring of specific ligands with the desired binding affinity.
- The combination of these two advantages—tuning of magnetic properties and surface versatility—makes ferrites useful and promising materials for applications where superparamagnetic behavior is required.
- Functionalized ferrite NPs, especially Fe_3O_4, are useful for removing a wide variety of heavy metals. In the case of cations, amino, carboxyl and thiol functional groups prevail as preferred candidates for metal uptake, although phosphonic and hydroxamic acids constitute promising ligands. Multifunctional ligands (synthetic and natural polymers) contribute to increase the stability and the adsorption capacity of the sorbent. At intermediate pH values, the tendency between metal-ligand affinities shows that for carboxyl and amino groups, the NPs are more selective toward hard Lewis acids, while for softer ligands like sulfur groups, the tendency is inverted.
- For removing arsenic, additional studies are warranted since controversy exists about the structure of the inner-sphere complexes and the nature of redox reactions at the interface. Also, the use of organic ligands to drive arsenic removal has not been exhausted yet.
- Most adsorption studies are limited to thermodynamic and kinetic analysis and the investigations of metal-binding interactions are supported by phenomenological models. But the mode of coordination and the geometry of the surface complexes are not clear and so detailed spectroscopic studies are still needed. Since this is a tough task due to the inherent difficulties for the achievement of a rigorous surface picture, the use of theoretical calculations could help in this regard.
- Organic dyes are preferentially adsorbed by ligand-decorated magnetic NPs. Composites with functional carbonaceous materials and grafting of smart polymers are promising lines of development.
- Spinel ferrites are useful materials for different advanced oxidation technologies, especially as composites with graphene-based materials due to the electronic and adsorptive properties of these carbon-based functional materials, which enhance the overall efficiency of the process.

Acknowledgements

The preparation of this chapter was partially supported by the CONACyT (Mexico) Projects 2013-05-231461, CB-2014-01-235840 and 2015-270810.

http://dx.doi.org/10.5772/67513

Author details

Oscar F. Odio[1,2] and Edilso Reguera[2]*

*Address all correspondence to: edilso.reguera@gmail.com

1 Universidad de La Habana, Instituto de Ciencia y Tecnología de Materiales, La Habana, Cuba

2 Instituto Politécnico Nacional, Centro de Investigación en Ciencia Aplicada y Tecnología Avanzada-Unidad Legaria, México

References

[1] Kalia S, Kango S, Kumar A, Haldorai Y, Kumari B, Kumar R. Colloid Polym. Sci. 2014;292(9):2025–2052.

[2] Wu L, Mendoza-Garcia A, Li Q, Sun S. Chem. Rev. 2016;116(18):10473–10512.

[3] Kharisov BI, Dias HVR, Kharissova OV. Arab. J. Chem. 2014. DOI: 10.1016/j.arabjc.2014.10.049.

[4] Su C. J. Hazard. Journal of hazardous materials. 2017;322(Pt A):48–84.

[5] Reddy DH, Lee SM. Adv. Colloid Interface Sci. 2013;201–202:68–93.

[6] Reddy DHK, Yun Y-S. Coordin. Chem. Rev. 2016;315:90–111.

[7] Mehta D, Mazumdar S, Singh SK. J. Water Process Eng. 2015;7:244–265.

[8] Laurent S, Forge D, Port M, Roch A, Robic C, Vander Elst L, Muller RN. Chem. Rev. 2008;108(6):2064–2110.

[9] Lu AH, Salabas EL, Schüth F. Angew. Chem. Int. Ed. 2007;46(8):1222–1244.

[10] Mathew DS, Juang R-S. Chem. Eng. J. 2007;129(1–3):51–65.

[11] Jang JT, Nah H, Lee JH, Moon SH, Kim MG, Cheon J. Angew. Chem. 2009;48(7):1234–1238.

[12] Albuquerque AS, Tolentino MVC, Ardisson JD, Moura FCC, De Mendona R, MacEdo WAA. Ceram. Int. 2012;38:2225–2231.

[13] Tahar LB, Basti H, Herbst F, Smiri LS, Quisefit JP, Yaacoub N, Grenèche JM, Ammar S. Mater. Res. Bull. 2012;47(9):2590–2598.

[14] Sorensen CM. Magnetism. In: Klabunde KJ, editor. Nanoscale Materials in Chemistry. New York: John Wiley & Sons; 2001. p. 169–221.

[15] Néel L. Ann. Geophys. 1949;5:99–136.

[16] Mohapatra J, Mitra A, Bahadur D, Aslam M. Cryst. Eng. Comm. 2013;15(3):524–532.

[17] Fernandes C, Pereira C, Fernández-García MP, Pereira AM, Guedes A, Fernández-Pacheco R, Ibarra A, Ibarra MR, Araújo JP, Freire C. J. Mater. Chem. C. 2014;2(29):5818.

[18] Artus M, Tahar LB, Herbst F, Smiri L, Villain F, Yaacoub N, Grenèche J-M, Ammar S, Fiévet F. J. Phys. Condens. Mat. 2011;23:506001.

[19] Dutta P, Pal S, Seehra MS, Shah N, Huffman GP. J. Appl. Phys. 2009;105:07B501.

[20] Yuan Y, Rende D, Altan CL, Bucak S, Ozisik R, Borca-Tasciuc D-A. Langmuir. 2012;28:13051–13059.

[21] Costo R, Morales MP, Veintemillas-Verdaguer S. J. Appl. Phys. 2015;117(6):064311.

[22] Jovanović S, Spreitzer M, Tramšek M, Trontelj Z, Suvorov D. J. Phys. Chem. C. 2014;118 (25):13844–13856.

[23] Daou TJ, Grenèche JM, Pourroy G, Buathong S, Derory A, Ulhaq-Bouillet C, Donnio B, Guillon D, Begin-Colin S. Chem. Mater. 2008;20(18):5869–5875.

[24] Odio OF, Lartundo-Rojas L, Santiago-Jacinto P, Martínez R, Reguera E. J. Phys. Chem. C. 2014;118:2776–2791.

[25] Aslibeiki B, Kameli P, Ehsani MH, Salamati H, Muscas G, Agostinelli E, Foglietti V, Casciardi S, Peddis D. J. Magn. Magn. Mater. 2016;399:236–244.

[26] Jia X, Chen D, Jiao X, He T, Wang H, Jiang W. J. Phys. Chem. C. 2008;112(4):911–917.

[27] Topkaya R, Kurtan U, Baykal A, Toprak MS. Ceram. Int. 2013;39(5):5651–5658.

[28] Vestal CR, Zhang ZJ. J. Am. Chem. Soc. 2003;125:9828–9833.

[29] Li Z, Chen H, Bao H, Gao M. Chem. Mater. 2004;16(8):1391–1393.

[30] Vestal CR, Zhang ZJ. Nano Lett. 2003;3:1739–1743.

[31] Batlle X, Pérez N, Guardia P, Iglesias O, Labarta A, Bartolomé F, García L, Bartolomé J, Roca A, Morales M. J. Appl. Phys. 2011;109(7):07B524-1–07B524-6.

[32] Pereira AM, Pereira C, Silva AS, Schmool DS, Freire C, Grenèche J-M, Araújo JP. J. Appl. Phys. 2011;109(11):114319–114324.

[33] Yang H, Hasegawa D, Takahashi M, Ogawa T. Appl. Phys. Lett. 2009;94(1):013103-1–013103-3.

[34] Odio OF, Lartundo-Rojas L, Palacios EG, Martínez R, Reguera E. Appl. Surf. Sci. 2016;386:160–177.

[35] Bishop KJ, Wilmer CE, Soh S, Grzybowski BA. Small. 2009;5(14):1600–1630.

[36] Peddis D, Cannas C, Musinu A, Ardu A, Orrù F, Fiorani D, Laureti S, Rinaldi D, Muscas G, Concas G, Piccaluga G. Chem. Mater. 2013;25:2–10.

[37] Dormann JL, Fiorani D, Tronc E. J. Magn. Magn. Mater. 1999;202:251–267.

[38] Tholence JL, Solid St. Commun. 1980;35(2):113–117.

[39] Shtrikman S, Wohlfarth EP, Phys. Lett. 1981;85(8–9):467–470.

[40] Singh V, Seehra MS, Bonevich J, J. Appl. Phys. 2009;105(7): 07B518.

[41] Dormann JL, Bessais L, Fiorani D, J. Phys. C. 1998;21(10):2015–2034.

[42] Seehra MS, Pisane KL, J. Phys. Chem. Solids. 2016;93:79–81.

[43] Yang L, Zhang Y, Liu X, Jiang X, Zhang Z, Zhang T, Zhang L. Chem. Eng. J. 2014;246:88–96.

[44] Roonasi P, Nezhad AY. Mater. Chem. Phys. 2015;172:143–149.

[45] Massart R, Cabuil V. J. Chim. Phys. PCB. 1987;84(7–8):967–973.

[46] Mascolo M, Pei Y, Ring T. Materials. 2013;6(12):5549–5567.

[47] Vadivel M, Babu RR, Arivanandhan M, Ramamurthi K, Hayakawa Y. RSC Adv. 2015;5 (34):27060–27068.

[48] Krishna Surendra M, Annapoorani S, Ansar EB, Harikrishna Varma PR, Ramachandra Rao MS. J. Nanopart. Res. 2014;16(12):2773.

[49] Zhang Y, Nan Z. Mater. Lett. 2015;149:22–24.

[50] Anirudhan T, Shainy F. J. Ind. Eng. Chem. 2015;32:157–166.

[51] Garza-Navarro MA, Torres-Castro A, García-Gutiérrez DI, Ortiz-Rivera L, Wang YC, González-González VA. J. Phys. Chem. C. 2010;114(41):17574–17579.

[52] Tran HV, Tran LD, Nguyen TN. Mater. Sci. Eng.: C. 2010;30(2):304–310.

[53] Yao Y, Yang Z, Zhang D, Peng W, Sun H, Wang S. Ind. Eng. Chem. Res. 2012;51:6044–6051.

[54] Yao Y, Cai Y, Lu F, Wei F, Wang X, Wang S. J. Hazard. Mater. 2014;270:61–70.

[55] Lingamdinne LP, Choi Y-L, Kim I-S, Chang Y-Y, Koduru JR, Yang J-K. RSC Adv. 2016;6:73776–73789.

[56] Pereira C, Pereira AM, Fernandes C, Rocha M, Mendes R, Fernández-García MP, Guedes A, Tavares PB, Grenèche J-M, Araújo JP, Freire C. Chem. Mater. 2012;24(8):1496–1504.

[57] Zhang Y, Shi Q, Schliesser J, Woodfield BF, Nan Z. Inorg. Chem. 2014;53(19):10463–10470.

[58] Verma S, Pravarthana D. Langmuir. 2011;27(21):13189–13197.

[59] Park J, An K, Hwang Y, Park JG, Noh HJ, Kim JY, Park JH, Hwang NM, Hyeon T. Nat. Mater. 2004;3(12):891–895.

[60] Park J, Lee E, Hwang NM, Kang M, Kim SC, Hwang Y, Park JG, Noh HJ, Kim JY, Park JH. Angew. Chem. 2005;117(19):2932–2937.

[61] Sun S, Zeng H, Robinson DB, Raoux S, Rice PM, Wang SX, Li G. J. Am. Chem. Soc. 2004;126(1):273–279.

[62] Yang C, Wu J, Hou Y. Chem. Comm. 2011;47(18):5130–5141.

[63] Silvestri A, Mondini S, Marelli M, Pifferi V, Falciola L, Ponti A, Ferretti AM, Polito L. Langmuir. 2016;32(28):7117–7126.

[64] Moriya M, Ito M, Sakamoto W, Yogo T. Cryst. Growth Des. 2009;9(4):1889–1893.

[65] Mondini S, Cenedese S, Marinoni G, Molteni G, Santo N, Bianchi CL, Ponti A. J. Colloid Interface Sci. 2008;322(1):173–179.

[66] Cai W, Wan J. J. Colloid Interface Sci. 2007;305(2):366–370.

[67] Zhang B, Tu Z, Zhao F, Wang J. Appl. Surf. Sci. 2013;266:375–379.

[68] Maity D, Chandrasekharan P, Si-Shen F, Xue J-M, Ding J. J. Appl. Phys. 2010;107 (9):09B310.

[69] Maity D, Kale SN, Kaul-Ghanekar R, Xue J-M, Ding J. J. Magn. Magn. Mater. 2009;321 (19):3093–3098.

[70] Deligöz H, Baykal A, Tanrıverdi EE, Durmus Z, Toprak MS. Mater. Res. Bull. 2012;47 (3):537–543.

[71] Gonçalves RH, Cardoso CA, Leite ER. J Mater Chem. 2010;20(6):1167–1172.

[72] Zhang C, Sui J, Li J, Tang Y, Cai W. Chem. Eng. J. 2012;210:45–52.

[73] Baldi G, Bonacchi D, Franchini MC, Gentili D, Lorenzi G, Ricci A, Ravagli C. Langmuir. 2007;23(7):4026–4028.

[74] Ji GB, Tang SL, Ren SK, Zhang FM, Gu BX, Du YW. J. Cryst. Growth. 2004;270(1–2): 156–161.

[75] Wu X, Wang W, Li F, Khaimanov S, Tsidaeva N, Lahoubi M. Appl. Surf. Sci. 2016;389: 1003–1011.

[76] Zong M, Huang Y, Ding X, Zhang N, Qu C, Wang Y. Ceram. Int. 2014;40(5):6821–6828.

[77] Meidanchi A, Akhavan O. Carbon. 2014;69:230–238.

[78] Rahman MM, Khan SB, Faisal M, Asiri AM, Alamry KA. Sensors Actuators B. 2012;171–172:932–937.

[79] Komarneni S, D'Arrigo MC, Leonelli C, Pellacani GC, Katsuki H. J. Am. Ceram. Soc. 1998;81(11):3041–3043.

[80] Bastami TR, Entezari MH, Kwong C, Qiao S. Front. Chem. Sci. Eng. 2014;8(3):378–385.

[81] Bai S, Shen X, Zhong X, Liu Y, Zhu G, Xu X, Chen K. Carbon. 2012;50:2337–2346.

[82] Ding Y, Zhu L, Wang N, Tang H. Appl. Catal. B. 2013;129:153–162.

[83] Zhang X, Feng M, Qu R, Liu H, Wang L, Wang Z. Chem. Eng. J. 2016;301:1–11.

[84] Aubery C, Solans C, Sanchez-Dominguez M. Langmuir. 2011;27(23):14005–14013.

[85] Cutting RS, Coker VS, Telling ND, Kimber RL, Pearce CI, Ellis BL, Lawson RS, van der Laan G, Pattrick RAD, Vaughan DJ, Arenholz E, Lloyd JR. Environ. Sci. Technol. 2010;44 (7):2577–2584.

[86] McCormick ML, Adriaens P. Environ. Sci. Technol. 2004;38(4):1045–1053.

[87] Kikukawa N, Takemori M, Nagano Y, Sugasawa M, Kobayashi S. J. Magn. Magn. Mater. 2004;284:206–214.

[88] Choodamani C, Nagabhushana GP, Ashoka S, Daruka Prasad B, Rudraswamy B, Chandrappa GT. J. Alloys Compd. 2013;578:103–109.

[89] Liu B, Li Q, Zhang B, Cui Y, Chen H, Chen G, Tang D. Nanoscale. 2011;3(5):2220–2226.

[90] Marin T, Montoya P, Arnache O, Calderon J. J. Phys. Chem. B. 2016;120(27):6634–6645.

[91] Bellusci M, Aliotta C, Fiorani D, La Barbera A, Padella F, Peddis D, Pilloni M, Secci D. J. Nanopart. Res. 2012;14(6):904.

[92] Duan H, Kuang M, Wang X, Wang YA, Mao H, Nie S. J. Phys. Chem. C. 2008;112 (22):8127–8131.

[93] Dai Q, Lam M, Swanson S, Yu RH, Milliron DJ, Topuria T, Jubert PO, Nelson A. Langmuir. 2010;26(22):17546–17551.

[94] Marcelo G, Pérez E, Corrales T, Peinado C. J. Phys. Chem. C. 2011;115(51):25247–25256.

[95] Tombácz E, Tóth IY, Nesztor D, Illés E, Hajdú A, Szekeres M, Vékás L. Colloids Surf. A. 2013;435:91–96.

[96] Cheng K, Peng S, Xu C, Sun S. J. Am. Chem. Soc. 2009;131(30):10637–10644.

[97] Das M, Mishra D, Maiti TK, Basak A, Pramanik P. Nanotechnology. 2008;19(41):415101.

[98] Rodovalho FL, Capistrano G, Gomes JA, Sodré FF, Chaker JA, Campos AFC, Bakuzis AF, Sousa MH. Chem. Eng. J. 2016;302:725–732.

[99] Dong A, Ye X, Chen J, Kang Y, Gordon T, Kikkawa JM, Murray CB. J. Am. Chem. Soc. 2010;133(4):998–1006.

[100] Wu Y, Guo J, Yang W, Wang C, Fu S. Polymer. 2006;47(15):5287–5294.

[101] Ge J, Hu Y, Biasini M, Dong C, Guo J, Beyermann WP, Yin Y. Chemistry. 2007;13 (25):7153–7161.

[102] Stöber W, Fink A, Bohn E. J. Colloid Interface Sci. 1968;26(1):62–69.

[103] Graf C, Vossen DLJ, Imhof A, van Blaaderen A. Langmuir. 2003;19(17):6693–6700.

[104] Gill CS, Price BA, Jones CW. J. Catal. 2007;251:145–152.

[105] Rocha M, Fernandes C, Pereira C, Rebelo SLH, Pereira MFR, Freire C. RSC Adv. 2015;5:5131–5141.

[106] Li G, Zhao Z, Liu J, Jiang G. J. Hazard. Mater. 2011;192(1):277–283.

[107] Lattuada M, Hatton TA. Langmuir. 2007; 23(4):2158–2168.

[108] Hood M, Mari M, Muñoz-Espí R. Materials. 2014;7(5):4057–4087.

[109] Gelbrich T, Feyen M, Schmidt AM. Macromolecules. 2006;39(9):3469–3472.

[110] Sun Y, Ding X, Zheng Z, Cheng X, Hu X, Peng Y. Eur. Polym. J. 2007;43(3):762–772.

[111] Li G-Y, Huang K-L, Jiang Y-R, Ding P, Yang D-L. Biochem. Eng. J. 2008;40(3):408–414.

[112] Zhang T, Ge J, Hu Y, Yin Y. Nano Lett. 2007;7(10):3203–3207.

[113] Huang SH, Chen DH. J. Hazard. Mater. 2009;163(1):174–179.

[114] Dolatkhah A, Wilson LD. ACS Appl. Mater. Interfaces. 2016;8(8):5595–5607.

[115] Wu W, He Q, Jiang C. Nanoscale Res. Lett. 2008;3(11):397–415.

[116] Zhao F, Tang WZ, Zhao D, Meng Y, Yin D, Sillanpää M. J. Water Proc. Eng. 2014;4:47–57.

[117] Zhao YG, Shen HY, Pan SD, Hu MQ. J. Hazard. Mater. 2010;182(1–3):295–302.

[118] Pan S, Shen H, Xu Q, Luo J, Hu M. J. Colloid Interface Sci. 2012;365(1):204–212.

[119] Ren Y, Abbood HA, He F, Peng H, Huang K. Chem. Eng. J. 2013;226:300–311.

[120] Ge F, Li MM, Ye H, Zhao BX. J. Hazard. Mater. 2012;211–212:366–372.

[121] Zhu Y, Hu J, Wang J. J. Hazard. Mater. 2012;221–222:155–161.

[122] Rutledge RD, Warner CL, Pittman JW, Addleman RS, Engelhard M, Chouyyok W, Warner MG. Langmuir. 2010;26(14):12285–12292.

[123] Zou Z, Wang S, Jia J, Xu F, Long Z, Hou X. Microchem. J. 2016;124:578–583.

[124] Zheng J, Cheng C, Fang W-J, Chen C, Yan R-W, Huai H-X, Wang C-C. Cryst. Eng. Comm. 2014;16(19):3960.

[125] Lai L, Xie Q, Chi L, Gu W, Wu D. J. Colloid Interface Sci. 2016;465:76–82.

[126] Xu Z, Hou Y, Sun S. J. Am. Chem. Soc. 2007;129(28):8698–8699.

[127] Dolci S, Ierardi V, Remskar M, Jagličić Z, Pineider F, Boni A, Pampaloni G, Veracini CA, Domenici V. J. Mater. Sci. 2013;48(3):1283–1291.

[128] Nishio K, Gokon N, Tsubouchi S, Ikeda M, Narimatsu H, Sakamoto S, Izumi Y, Abe M, Handa H. Chem. Lett. 2006;35(8):974–975.

[129] Soler MA, Lima EC, Nunes ES, Silva FL, Oliveira AC, Azevedo RB, Morais PC. J. Phys. Chem. A. 2011;115(6):1003–1008.

[130] Maurizi L, Bisht H, Bouyer F, Millot N. Langmuir. 2009;25(16):8857–8859.

[131] Daou TJ, Begin-Colin S, Grenèche JM, Thomas F, Derory A, Bernhardt P, Legaré P, Pourroy G. Chem. Mater. 2007;19(18):4494–4505.

[132] Hatakeyama M, Kishi H, Kita Y, Imai K, Nishio K, Karasawa S, Masaike Y, Sakamoto S, Sandhu A, Tanimoto A, Gomi T, Kohda E, Abe M, Handa H. J. Mater. Chem. 2011;21 (16):5959.

[133] Wilson D, Langell MA. Appl. Surf. Sci. 2014;303:6–13.

[134] Palchoudhury S, An W, Xu Y, Qin Y, Zhang Z, Chopra N, Holler RA, Turner CH, Bao Y. Nano Lett. 2011;11(3):1141–1146.

[135] Rath SS, Sinha N, Sahoo H, Das B, Mishra BK. Appl. Surf. Sci. 2014;295:115–122.

[136] Lin CL, Lee CF, Chiu WY. J. Colloid Interface Sci. 2005;291(2):411–420.

[137] Aslam M, Schultz EA, Sun T, Meade T, Dravid VP. Cryst. Growth Des. 2007;7(3):471–475.

[138] Sathish S, Balakumar S. Mater. Chem. Phys. 2016;173:364–371.

[139] Hua M, Zhang S, Pan B, Zhang W, Lv L, Zhang Q. J. Hazard. Mater. 2012;211–212:317–331.

[140] Gómez-Pastora J, Bringas E, Ortiz I. Chem. Eng. J. 2014;256:187–204.

[141] Järup L. Br. Med. Bull. 2003;68(1):167–182.

[142] Shen H, Pan S, Zhang Y, Huang X, Gong H. Chem. Eng. J. 2012;183:180–191.

[143] Zhao D, Gao X, Wu C, Xie R, Feng S, Chen C. Appl. Surf. Sci. 2016;384:1–9.

[144] Xin X, Wei Q, Yang J, Yan L, Feng R, Chen G, Du B, Li H. Chem. Eng. J. 2012;184:132–140.

[145] Tan Y, Chen M, Hao Y. Chem. Eng. J. 2012;191:104–111.

[146] Jainae K, Sukpirom N, Fuangswasdi S, Unob F. J. Ind. Eng. Chem. 2015;23:273–278.

[147] Zhao F, Repo E, Sillanpää M, Meng Y, Yin D, Tang WZ. Ind. Eng. Chem. Res. 2015;54:1271–1281.

[148] Liu Y, Fu R, Sun Y, Zhou X, Baig SA, Xu X. Appl. Surf. Sci. 2016;369:267–276.

[149] Mahdavian AR, Mirrahimi MA-S. Chem. Eng. J. 2010;159(1–3):264–271.

[150] Wang H, Chen QW, Chen J, Yu BX, Hu XY. Nanoscale. 2011;3(11):4600–4603.

[151] Wang Z, Xu J, Hu Y, Zhao H, Zhou J, Liu Y, Lou Z, Xu X. J. Taiwan Inst. Chem. Eng. 2016;60:394–402.

[152] Viltužnik B, Košak A, Zub YL, Lobnik A. J. Sol-Gel Sci. Technol. 2013;68(3):365–373.

[153] Zargoosh K, Abedini H, Abdolmaleki A, Molavian MR. Ind. Eng. Chem. Res. 2013;52:14944–14954.

[154] Guo B, Deng F, Zhao Y, Luo X, Luo S, Au C. Appl. Surf. Sci. 2014;292:438–446.

[155] Yantasee W, Warner CL, Sangvanich T, Addleman RS, Carter TG, Wiacek RJ, Fryxell GE, Timchalk C, Warner MG. Environ. Sci. Technol. 2007;41:5114–5119.

[156] Claudio ES, Godwin HA, Magyar JS. Fundamental Coordination Chemistry, Environmental Chemistry, and Biochemistry of Lead(II). In: Karlin KD, editor. Progress in Inorganic Chemistry, Volume 51. New York: John Wiley & Sons; 2003. p. 1–144.

[157] Liu C-H, Chuang Y-H, Chen T-Y, Tian Y, Li H, Wang M-K, Zhang W. Environ. Sci. Technol. 2015;49(13):7726–7734.

[158] Su C, Puls RW. Water Air Soil Poll. 2008;193(1–4):65–78.

[159] Lim SF, Zheng YM, Chen JP. Langmuir. 2009;25(9):4973–4978.

[160] Zhang S, Li XY, Chen JP. J. Colloid Interface Sci. 2010;343(1):232–238.

[161] Penke YK, Anantharaman G, Ramkumar J, Kar KK. RSC Adv. 2016;6:55608–55617.

[162] Peng B, Song T, Wang T, Chai L, Yang W, Li X, Li C, Wang H. Chem. Eng. J. 2016;299:15–22.

[163] Bhaumik M, Leswifi TY, Maity A, Srinivasu VV, Onyango MS. J. Hazard. Mater. 2011;186(1):150–159.

[164] Ai L, Zhang C, Chen Z. J. Hazard. Mater. 2011;192(3):1515–1524.

[165] Ou J, Mei M, Xu X. J. Solid State Chem. 2016;238:182–188.

[166] Zhang S, Dong Y, Yang Z, Yang W, Wu J, Dong C. Chem. Eng. J. 2016;304:325–334.

[167] Yang Q, Choi H, Al-Abed SR, Dionysiou DD. Appl. Catal. B. 2009;88:462–469.

[168] Guan YH, Ma J, Ren YM, Liu YL, Xiao JY, Lin Lq, Zhang C. Water Res. 2013;47:5431–5438.

[169] Zhang T, Zhu H, Croué J-P. Environ. Sci. Technol. 2013;47(6):2784–2791.

[170] Yan J, Lei M, Zhu L, Anjum MN, Zou J, Tang H. J. Hazard. Mater. 2011;186:1398–1404.

[171] Jumeri FA, Lim HN, Ariffin SN, Huang NM, Teo PS, Fatin SO, Chia CH, Harrison I. Ceram. Int. 2014;40:7057–7065.

[172] Fu Y, Chen H, Sun X, Wang X. Appl. Catal. B. 2012;111–112:280–287.

[173] Haw C, Chiu W, Abdul Rahman S, Khiew P, Radiman S, Abdul Shukor R, Hamid MAA, Ghazali N. New J. Chem. 2016;40:1124–1136.